Cranial Nerves II–VI

10

J. Matthew Debnam

The five cranial nerves (CNs) of the orbit relay important motor and sensory information about orbital muscle movement, vision, and facial sensation. These cranial nerves include the optic nerve (CN II), oculomotor nerve (CN III), trochlear nerve (CN IV), trigeminal nerve (CN V), and abducens nerve (CN VI). Lesions may arise within the nerve, such as an optic nerve glioma or from the nerve sheath, e.g., meningiomas and schwannomas. Other primary and secondary tumors can spread along the nerves, including perineural tumor spread, leptomeningeal disease, and neurolymphomatosis. Infection and other conditions such as idiopathic orbital inflammation and IgG4-related disease can also involve these CNs. Thus, imaging plays an important role in defining the presence and extent of disease and refining the differential diagnosis.

The imaging modalities used to evaluate the CNs include CT, MRI, and PET/CT. CT is used to assess the bony neural foramen for widening and destruction. MRI visualizes enhancing lesions of the CNs due to a superior contrast resolution. Both MRI and PET/CT provide important information for treatment planning and response.

The purpose of this chapter is to describe the demographics and imaging appearance of common and uncommon malignancies and tumor mimics that involve the CNs. This is accomplished with a review of the disease background, clinical presentation, and imaging features on various modalities. This chapter should provide the radiologist with a means to narrow their differential diagnosis when evaluating CN lesions. Lesions affecting the orbital CNs that occur in the skull base, sinonasal cavity, pituitary gland, cavernous sinus, and brain including the optic radiations are discussed in other chapters.

J. M. Debnam (✉)
Department of Neuroradiology, Division of Diagnostic Imaging, The University of Texas MD Anderson Cancer Center, Houston, TX, USA
e-mail: matthew.debnam@mdanderson.org

Orbital Cranial Nerve Anatomy

CN II (Optic Nerve)

Figures 10.1a and b, 10.2a, and 10.4 demonstrate the course of the optic nerve.

- Carries **visual information** from the globe to the visual cortex.
- **Axons are part of the white-matter tract; myelinated by oligodendrocytes**.
- Surrounded by subarachnoid space and covered by meninges.
  - **Prone to gliomas and meningiomas**.
- **Divided into four segments**: intraocular, intraorbital, intracanalicular, and prechiasmatic.
- Optic nerve emerges from the posterior globe.
- Exits the orbit via the **optic canal**.
- Bilateral optic nerves join to form the **optic chiasm**.
- **Nasal (medial) fibers of the optic nerves decussate (cross) in the optic chiasm; temporal (lateral) fibers do not cross**.
- Fibers from the optic chiasm travel in a posterolateral direction to the **lateral geniculate body**.
- Optic radiations originate in the lateral geniculate nucleus and travel posteriorly to reach the **primary visual cortex in the occipital lobe** (see Chap. 9 for further details).

CN III (Oculomotor Nerve)

Figures 10.1c, 10.2b, 10.3, and 10.4 demonstrate the course of the oculomotor nerve.

- Provides **motor function** to the **superior rectus, inferior rectus, and medial rectus muscles, the inferior oblique muscles, and the levator palpebrae superioris muscles**.

J. M. Debnam (ed.), *Imaging Atlas of Ophthalmic Tumors and Diseases*, https://doi.org/10.1007/978-3-031-17479-7_10

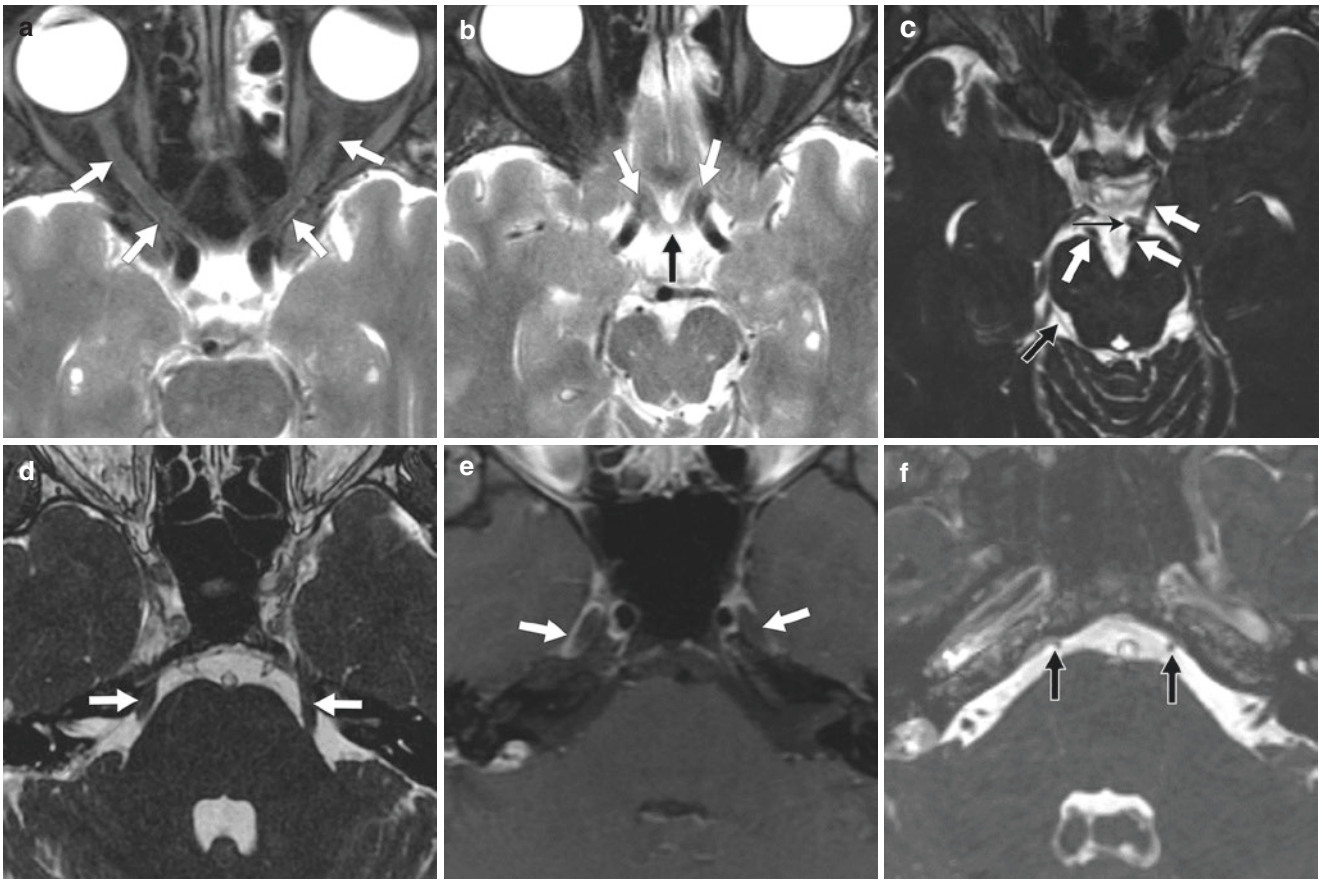

Fig. 10.1 MRI of cranial nerves II through VI. (**a**) Optic nerve extending posteriorly from the globe to the optic canal (arrows). (**b**) Prechiasmatic optic nerves (white arrows) before joining to form the optic chiasm (black arrow). (**c**) Oculomotor nerves (white arrows) emerge from the cerebral peduncle and course into the interpeduncular cistern. Note the left oculomotor nerve coursing inferior to the left posterior cerebral artery (thin black arrow). Right trochlear nerve in the ambient cistern (black arrow). (**d**) Trigeminal nerve roots (arrows) in the prepontine cistern. (**e**) Bilateral Meckel's caves (arrows) are conduits for the trigeminal nerves and house the trigeminal (Gasserian) ganglia. (**f**) Abducens nerves in the prepontine cistern (arrows)

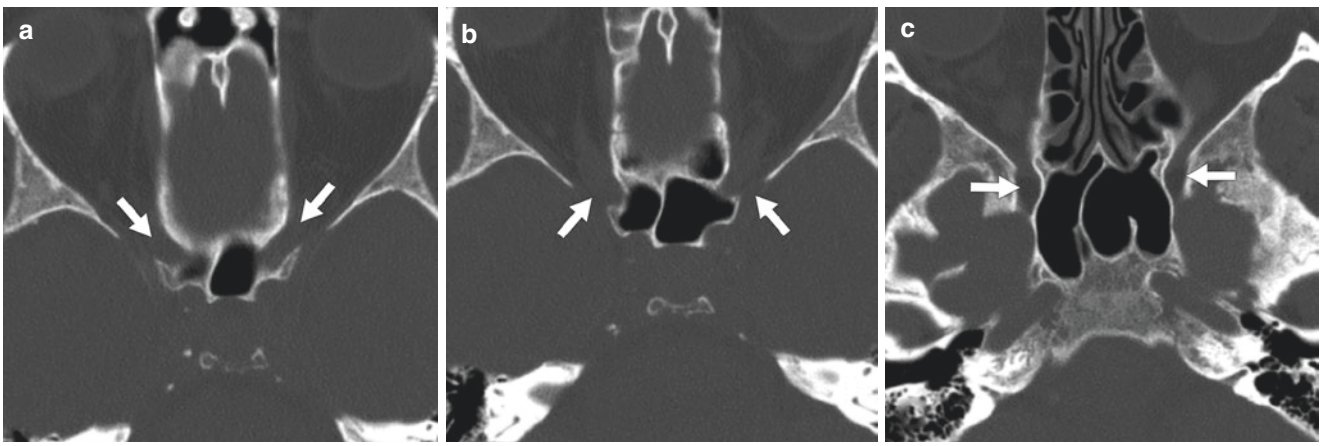

Fig. 10.2 CT images of the orbital and skull base foramina. (**a**) Optic canals (arrows). (**b**) Superior orbital fissures (arrows). (**c**) Foramen rotundum (arrows). (**d**) Pterygopalatine fossae (arrows). (**e**) Inferior orbital fissures (arrows). (**f**) Foramen ovale (arrows)

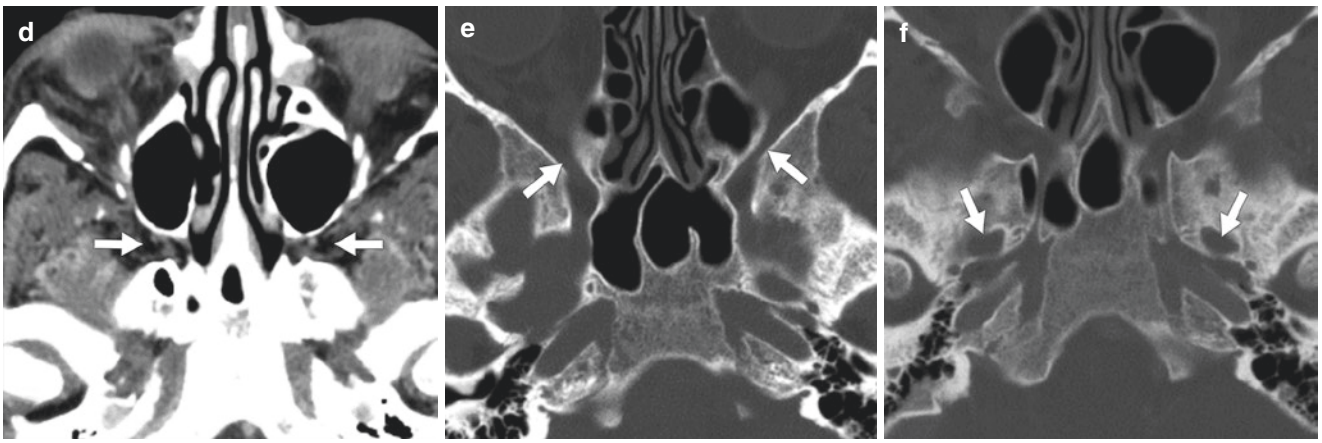

Fig. 10.2 (continued)

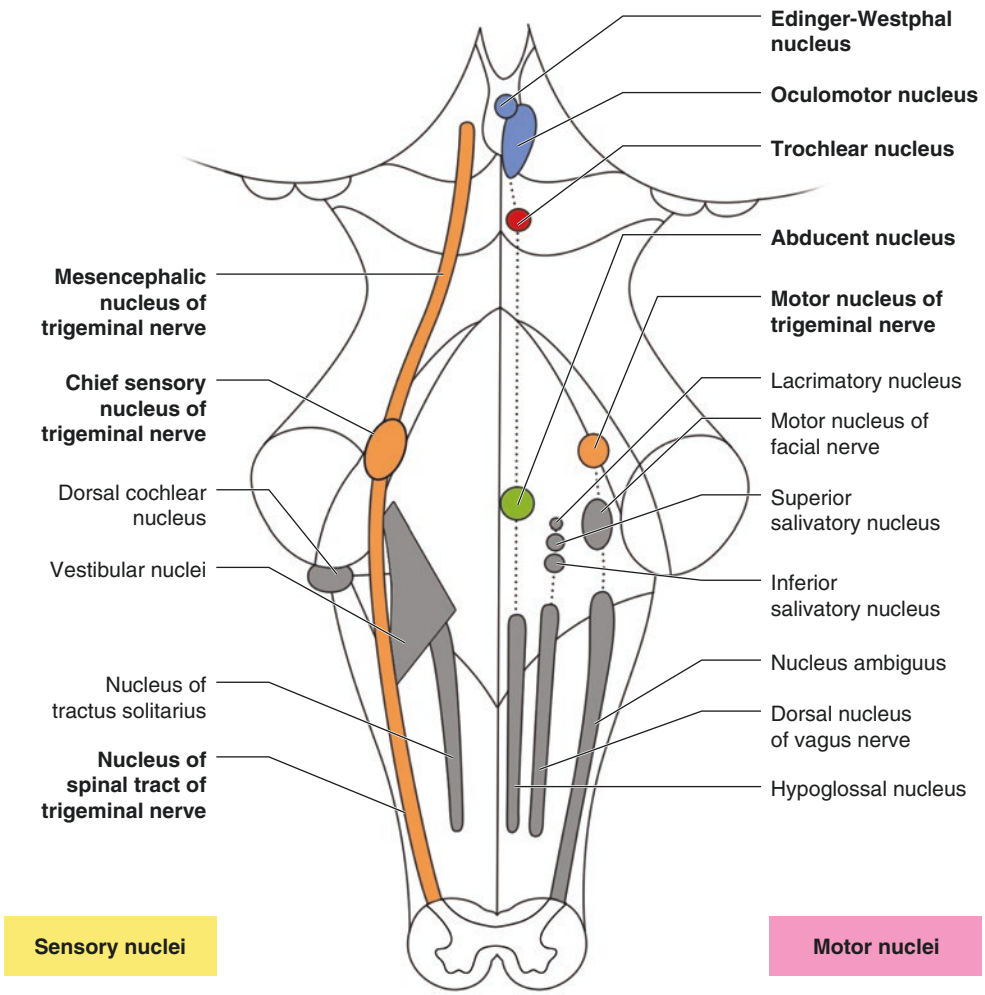

Fig. 10.3 Drawing of the brainstem and cranial nerve nuclei. Motor nuclei are on the right and sensory nuclei on the left

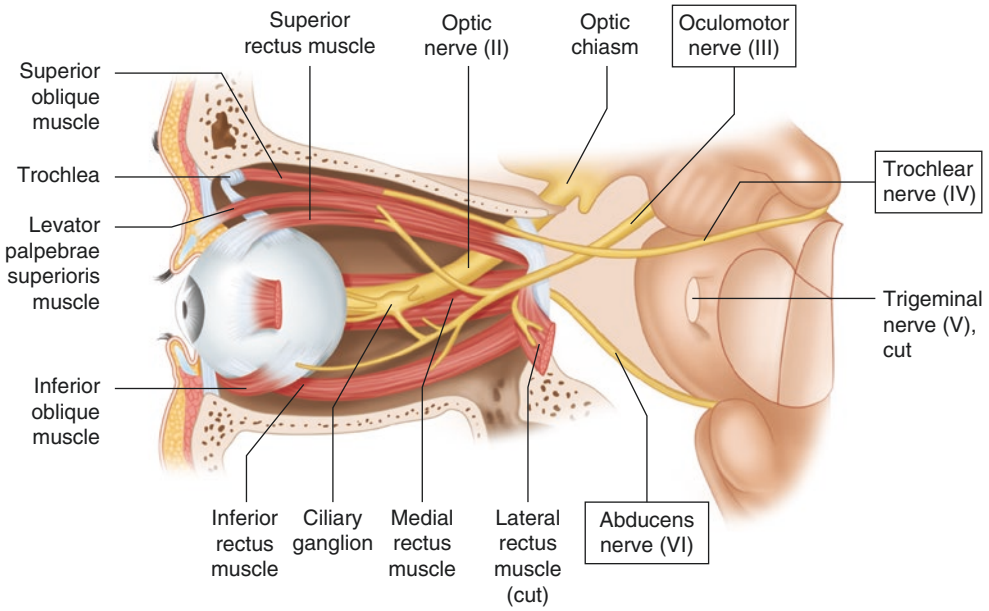

Fig. 10.4 Schematic drawing of the optic, oculomotor, trochlear, and abducens nerves. The optic nerve courses posteriorly from the globe to the visual cortex. The oculomotor nerve emerges from the midbrain, courses through the lateral wall of the cavernous sinus, and then through the superior orbital fissure to enter the orbit. The trochlear nerve emerges from the posterior midbrain, extends around the cerebral peduncles, through the lateral wall of the cavernous sinus, and then through the superior orbital fissure into the orbit. The abducens nerve emerges at the pontomedullary junction and courses through the prepontine cistern, the cavernous sinus inferolateral to the internal carotid artery, and through the superior orbital fissure to enter the orbit

- The **oculomotor nucleus** is located in the midbrain anterior to the periaqueductal grey matter.
- **Parasympathetic fibers** that innervate the pupillary constrictor and ciliary muscles originate in the **Edinger-Westphal nucleus,** which is located posterior to the oculomotor nucleus.
  - **Pupillary light reflex and lens accommodation response.**
- Emerges from the **medial aspect of the cerebral peduncle into the interpeduncular cistern and traverses the perimesencephalic cistern**.
- Courses anteriorly **below the posterior cerebral artery** and **above the superior cerebellar artery**.
- Enters the **cavernous sinus** in the **lateral wall as the most superior nerve**.
- Enters the orbit via the **superior orbital fissure**.
- **Superior division** gives branches to the superior rectus and levator palpebrae superioris muscles (superior rectus-levator complex).
- **Inferior division** innervates the inferior and medial rectus and inferior oblique muscles.

CN IV (Trochlear Nerve)

Figures 10.1c, 10.2b, 10.3, and 10.4 demonstrate the course of the trochlear nerve.

- Innervates the **superior oblique muscle**.
- **Nucleus lies in the midbrain, anterior to the periaqueductal grey matter**.
- **Fibers course posteriorly in the midbrain, decussate posterior to the periaqueductal grey matter, and then exit the pons below the inferior colliculus**.
- Runs anteriorly **around the cerebral peduncles in the ambient cistern**.
- Courses along the free margin of the tentorium and pierces the dura between the free and attached edges of the tentorium.
- **Passes into the lateral wall of the cavernous sinus**.
  - **Located inferior to the oculomotor nerve (CN III) and above the ophthalmic division of the trigeminal nerve (CN V_1)**.
- Enters the orbit via the **superior orbital fissure**.
- In the orbit, it extends superiorly and medially above the superior rectus-levator complex to innervate the superior oblique muscle.

CN V (Trigeminal Nerve)

Figures 10.1d and e, 10.2b–f, 10.3, and 10.5 demonstrate the course of the trigeminal nerve.

- Largest of the cranial nerves; contains sensory and motor roots.

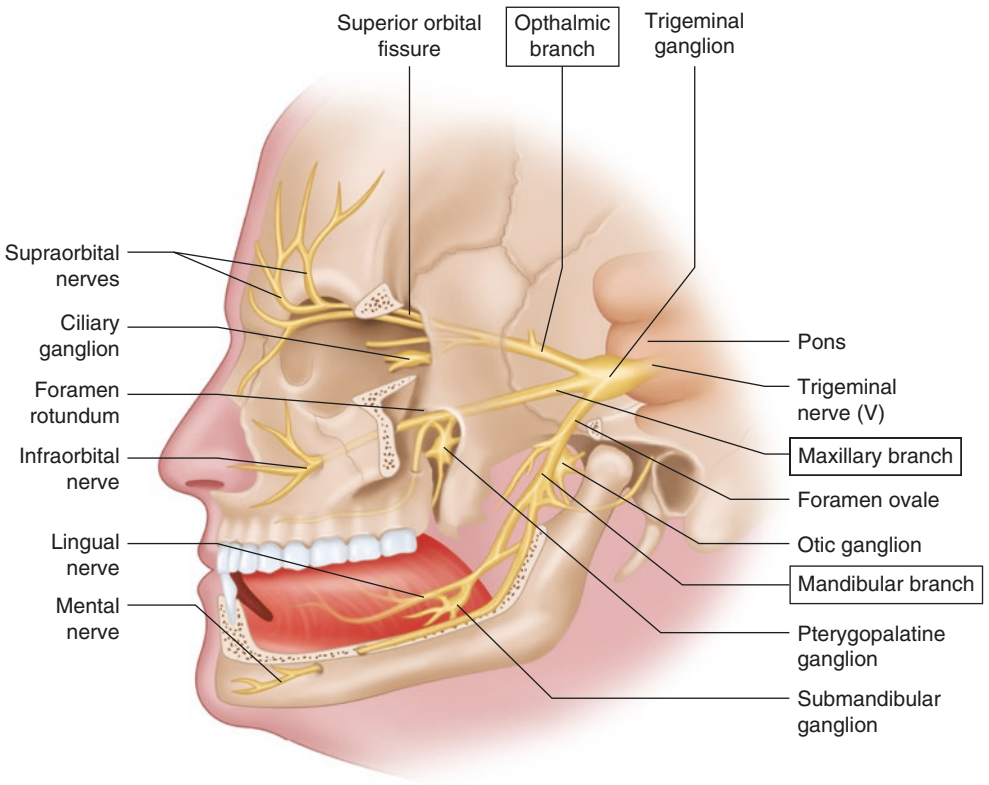

Fig. 10.5 Schematic drawing of the trigeminal nerve (CN V). The nerve root emerges from the lateral pons and passes through the prepontine cistern into Meckel's cave, where the trigeminal (Gasserian) ganglion is located. The nerve splits into three divisions. The ophthalmic (V_1) nerve courses through the lateral wall of the cavernous sinus, enters the orbit via the superior orbital fissure, and a branch extends to the face via the supraorbital foramen. The maxillary (V_2) nerve passes through the lateral wall of the cavernous sinus, exits the skull base via the foramen rotundum, enters the pterygopalatine fossa and inferior orbital fissure, and extends to the mid-face via the infraorbital canal and foramen. The mandibular (V_3) nerves course inferiorly through the foramen ovale and branches into the lingual and inferior alveolar nerves

- **Supplies sensations to the face and mucous membranes, and motor function for the muscles of mastication**.
- Four trigeminal nuclei: mesencephalic nucleus, chief sensory nucleus, nucleus of the spinal tract, and motor nucleus.
  - Nuclei extend from the midbrain inferiorly to the upper medulla.
- The trigeminal nerve root **exits the brainstem from the lateral pons. It passes through the prepontine cistern into a dural recess at the petrous apex (Meckel's cave) where the trigeminal ganglion (Gasserian ganglion) is located**.
- Nerve splits into **three divisions**: ophthalmic (V_1), maxillary (V_2), and mandibular (V_3) nerves.
- **V_1 and V_2 course in the lateral wall of the cavernous sinus**.
- **V_1 enters the orbit through the superior orbital fissure**.
  - Three terminal branches, each passing separately into the orbit via the superior orbital fissure.
  - The **lacrimal nerve** innervates the lacrimal gland and a portion of the upper eyelid.
  - The **frontal nerve** exits through the supraorbital foramen to provide sensory innervation to the upper face and scalp.
  - The **nasociliary nerve** provides sensory innervation to the eyelids, conjunctiva, cornea, ethmoid air cells, and nasal cavity mucosa.
- **V_2 exits the skull base via the foramen rotundum and passes through the pterygopalatine fossa.**
- **V_2 enters the orbit through the inferior orbital fissure, passing within the infraorbital canal, and extends to the face via the infraorbital foramen.** Provides sensory innervation of the mid-face.
- **V_3 exits the skull base through the foramen ovale** into the infratemporal fossa and **branches into the lingual** (sensation of the anterior 2/3 of the tongue) and **inferior alveolar nerves** (sensation of the lower teeth and chin; motor fibers to the muscles of mastication).

CN VI (Abducens Nerve)

Figures 10.1f, 10.2b, 10.3, and 10.4 demonstrate the course of the abducens nerve.

- **Innervates the lateral rectus muscle**.
- A**bducens nucleus** is located in the **dorsal pons just inferior to the floor of the fourth ventricle**.
- The abducens nerve emerges at the **pontomedullary junction and courses through the prepontine cistern**.
- **Most medial of the nerves exiting the brainstem** at the pontomedullary junction (facial nerve [CN VII] and vestibulocochlear nerve [CN VIII] are more lateral).
- Courses anteriorly through the **prepontine cistern** toward the clivus and runs superiorly along the clivus in a fibrous sheath named Dorello's canal.
- Courses over the medial petrous apex toward the cavernous sinus.
- Lies in the central venous portion of the cavernous sinus inferolateral to the internal carotid artery.
- Enters the orbit via the **superior orbital fissure** to innervate the lateral rectus muscle.

Optic Nerve Sheath Meningioma

Figures 10.6, 10.7, and 10.8 show cases of optic nerve sheath meningiomas.

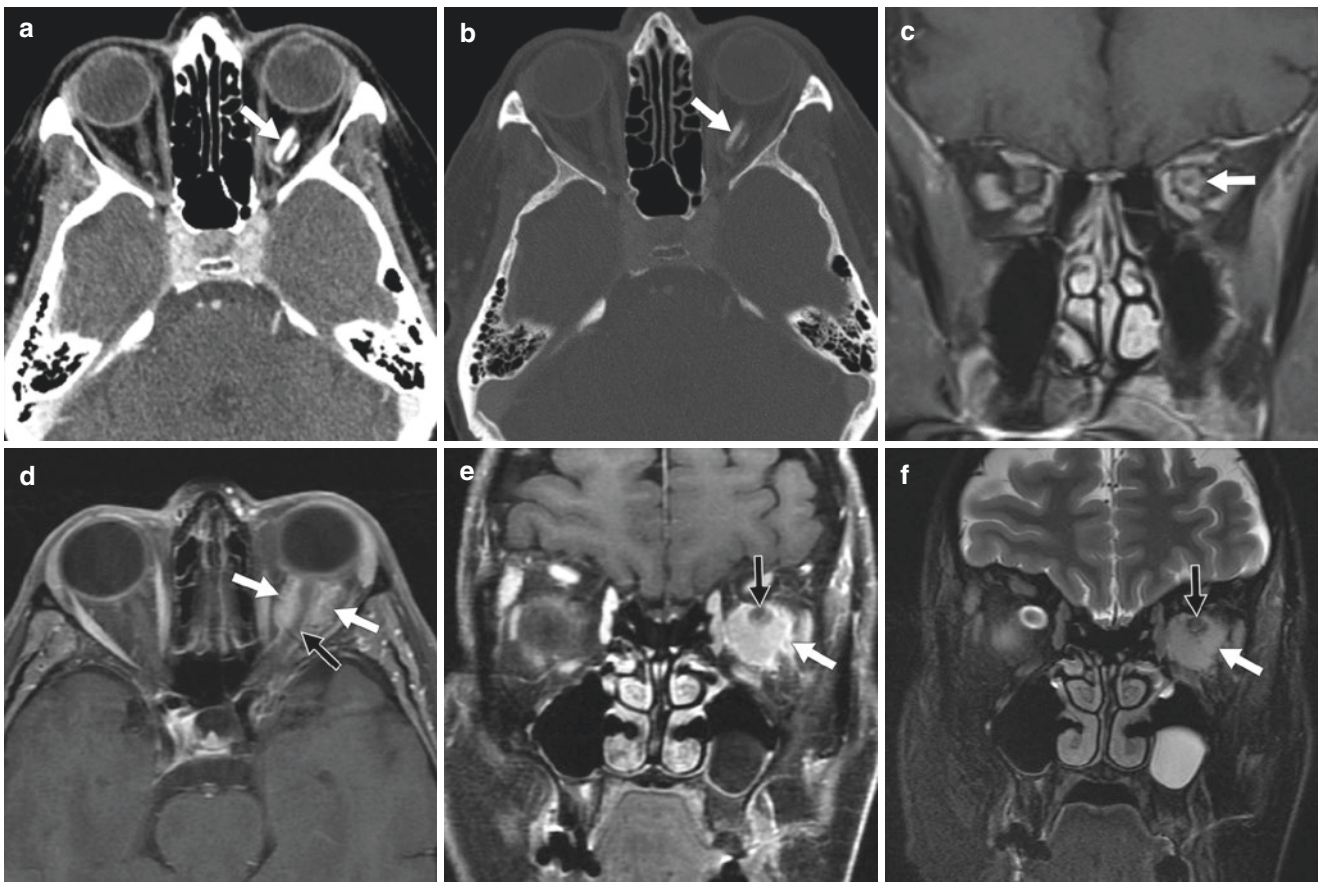

Fig. 10.6 (**a**–**c**) A 57-year-old female with left visual disturbance due to an optic nerve sheath meningioma. (**a**) Axial CT with contrast, soft tissue window shows **tram-track calcification** (arrow) **around the left optic nerve**. (**b**) Axial CT with contrast, bone window shows the **tram-track calcification** (arrow). (**c**) Coronal T1 post-contrast MRI shows **homogeneous enhancement of the meningioma** (arrow) **surrounding the optic nerve**. (**d**–**f**) A 36-year-old female with papilledema detected on routine eye examination. (**d**, **e**) Axial and coronal T1 post-contrast MRI with fat saturation shows **homogeneous enhancement of a left optic nerve sheath meningioma** (white arrows) **located eccentrically surrounding the optic nerve** (black arrows). (**f**) Coronal T2 MRI with fat saturation shows a **hyperintense appearance of the meningioma** (white arrow) **surrounding the optic nerve** (black arrow)

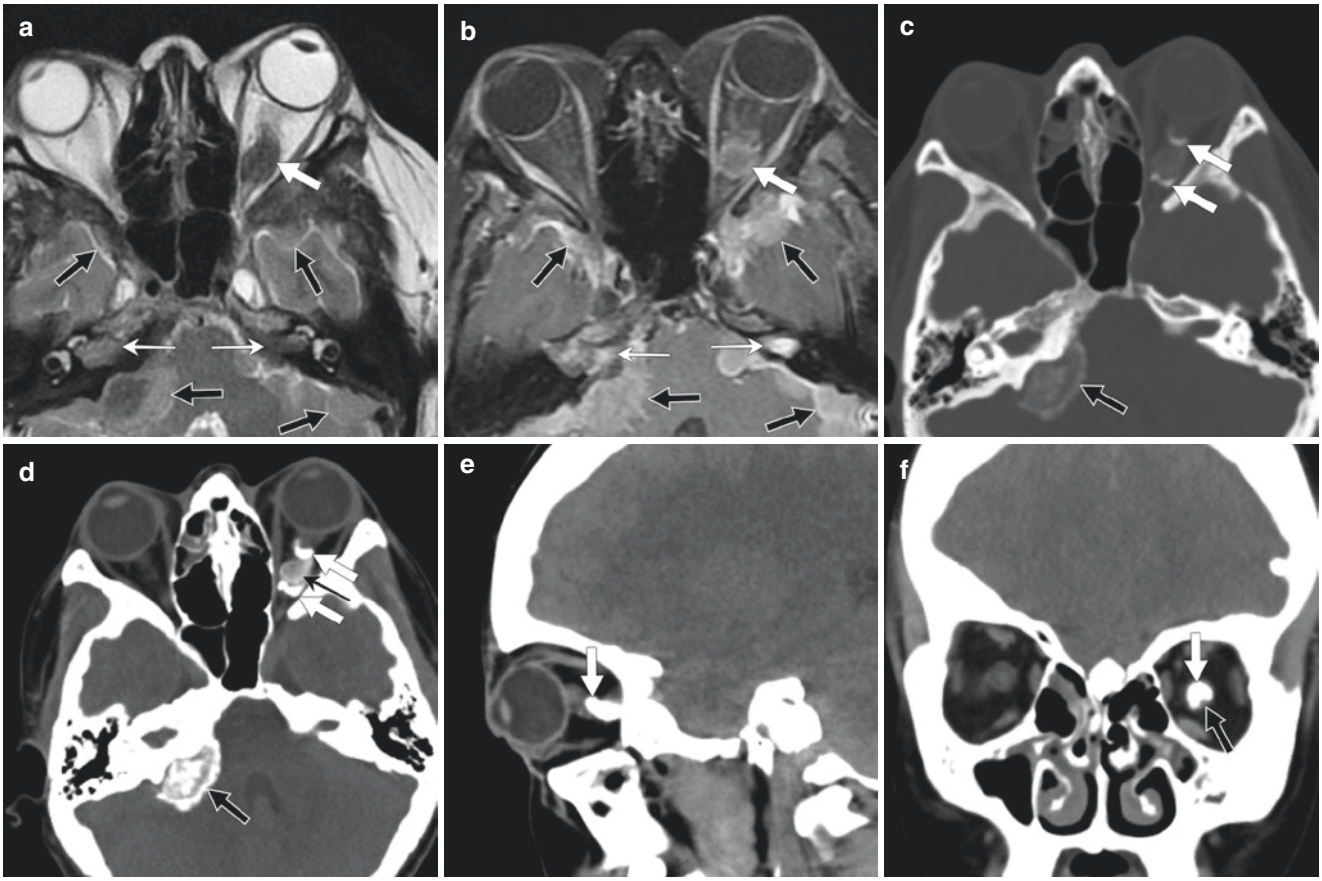

Fig. 10.7 A 28-year-old female with a history of NF-2 presented with headaches and papilledema due to an optic nerve sheath meningioma. (**a**) Axial T2 MRI with fat saturation shows a **hypointense left optic nerve mass** (white arrow). **Note multiple intracranial meningiomas** (black arrows) and **bilateral vestibular schwannomas** (thin white arrows). (**b**) Axial T1 post-contrast MRI with fat saturation shows **enhancement of the optic nerve sheath meningioma** (white arrow), **the intracranial meningiomas** (black arrow), **and bilateral vestibular schwannomas** (thin white arrows). (**c**) Axial T1 CT with contrast, bone window shows **calcifications associated with the left optic nerve meningioma** (white arrows) **and the right posterior fossa meningioma** (black arrow). (**d**) Axial CT with contrast, soft tissue window shows **calcification of the optic nerve sheath meningioma** (white arrows) and **enhancement of the noncalcified portion of the meningioma** (thin black arrow). **Note the calcification and enhancement of the right posterior fossa meningioma** (black arrow). (**e**, **f**) Sagittal and coronal CT with contrast, soft tissue windows shows **calcification of the left optic nerve sheath meningioma** (white arrows) **surrounding the optic nerve** (black arrow)

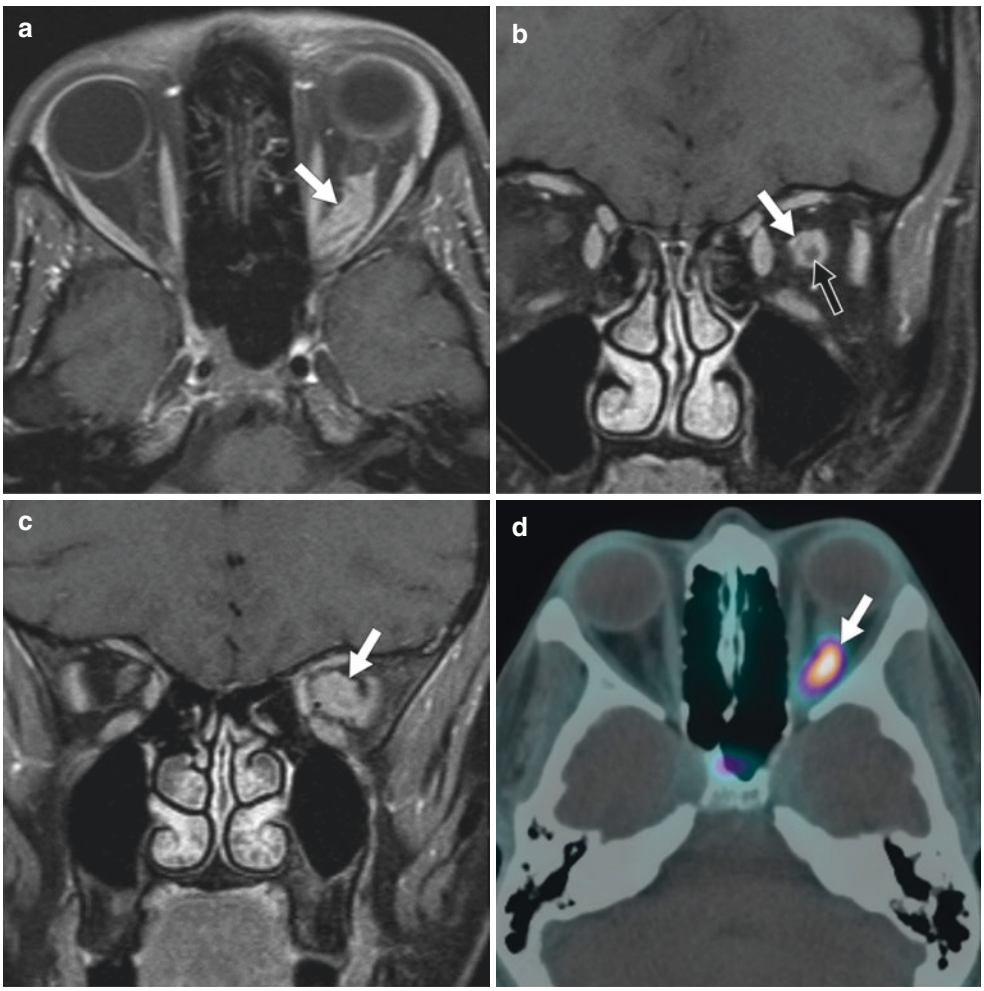

Fig. 10.8 A 28-year-old female with left vision loss over the past year. (**a**) Axial T1 post-contrast MRI with fat saturation shows a **homogeneously enhancing mass associated with the left optic nerve** (arrow). (**b**) Coronal T1 post-contrast MRI with fat saturation shows **homogeneous enhancement of the mass** (white arrow) **surrounding the optic nerve** (black arrow), suggestive of a meningioma. (**c**) Coronal T1 post-contrast MRI with fat saturation through the posterior orbit shows **homogeneous enhancement of the mass** (arrow) **without visualization of the optic nerve,** raising concern that the mass could be an optic nerve glioma. (**d**) ^{68}Ga-DOTATATE PET/CT shows **avidity of the optic nerve meningioma** (arrow)

Background

- **Benign tumor of the optic nerve sheath arising from arachnoid cap cells**.
- Located **inside the dura** [1].
- Associated with **neurofibromatosis type II (NF-2)** [2].

Presentation

- **Mean age at presentation: 40 years** [2].
- **Up to 25% present in children; tend to be more aggressive** [3].
- **Female predilection** [2].
- **Usually unilateral** [2, 4].
- Bilateral involvement can occur with tumor extension to the optic chiasm and contralateral nerve [2].
- **Symptoms**: vision loss, proptosis [3].

Imaging

- **Tubular (65%), exophytic (25%), or fusiform (10%)** [2].
- **Tram-track sign:** appearance of the enhancing meningioma as it surrounds the non-enhancing optic nerve in the axial and sagittal oblique planes [5].
- In the coronal plane, enhancement of the meningioma **surrounds the optic nerve** [6].
- **Optic nerve meningiomas in the optic canal can cause widening or hyperostosis** [2].

CT

- **Isointense to the optic nerve with homogeneous enhancement**.
- Calcifications form a "**sleeve-like case**" around the optic nerve [2].
- Useful to detect **calcification** and evaluate the optic nerve canal [3].

MRI

- **T1 iso- to hypointense** to the optic nerve with **homogeneous enhancement**.
- **T2 iso- to hyperintense** to the optic nerve [7, 8].

PET/CT

- **^{68}Ga-DOTATATE PET/CT** has been reported to confirm the presence of optic sheath meningioma [9, 10].
- ^{68}Ga-DOTATATE is a radiolabeled somatostatin receptor ligand.
- Meningiomas have overexpression of somatostatin receptors.
- Neuroendocrine and pituitary tumors can also be ^{68}Ga-DOTATATE avid [9].

Key Points

- Review the orbital apex and optic canal.
- **Tram-track sign** can be seen in other lesions such as perioptic lymphoma, leukemia, metastases, idiopathic orbital inflammation, sarcoidosis, Erdheim-Chester disease, perioptic hemorrhage, and optic neuritis.

Optic Nerve Glioma

Figures 10.9, 10.10, and 10.11 show cases of optic nerve gliomas.

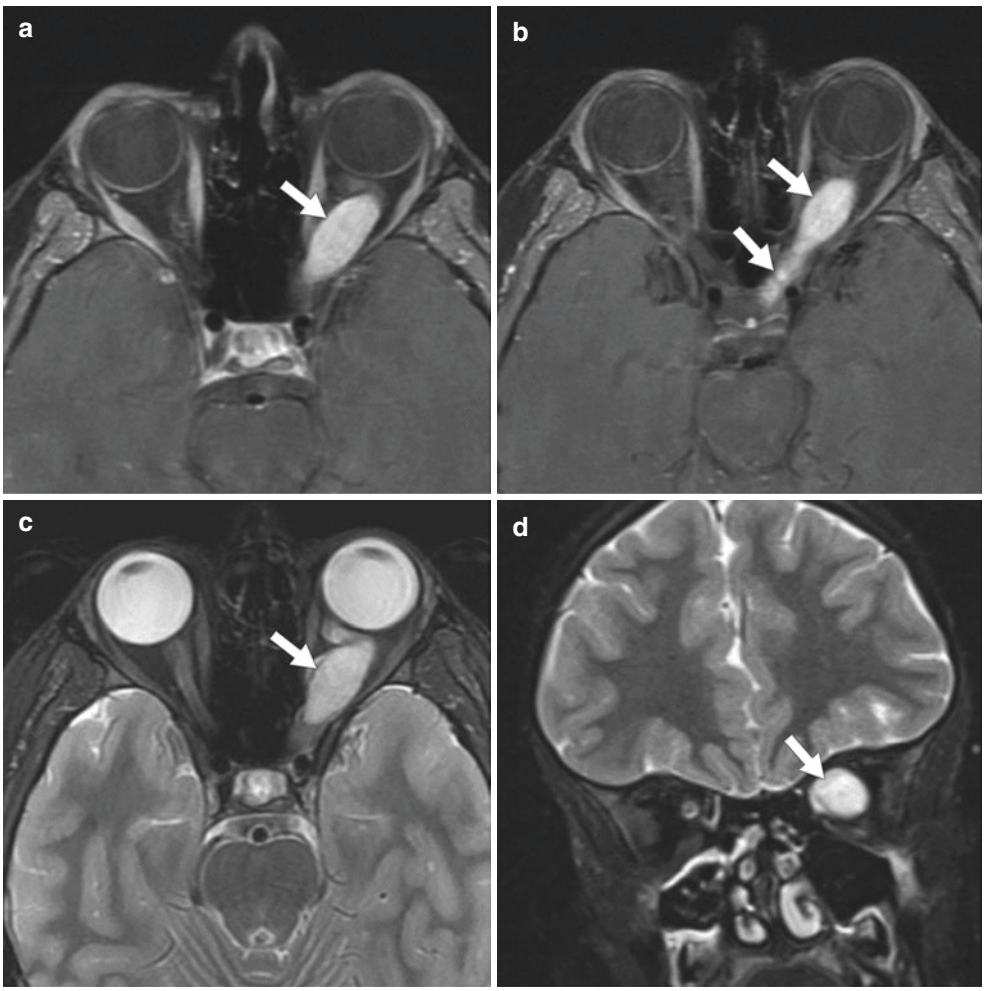

Fig. 10.9 A 10-year-old female with decreased vision in the left eye due to an optic nerve glioma. (**a**, **b**) Axial T1 post-contrast MRI with fat saturation shows a **homogeneously enhancing tubular mass involving the left intraocular, canalicular, and prechiasmatic optic nerve segments** (arrows). (**c**, **d**) Axial and coronal T2 MRI with fat saturation show a **hyperintense appearance of the optic nerve glioma** (arrows)

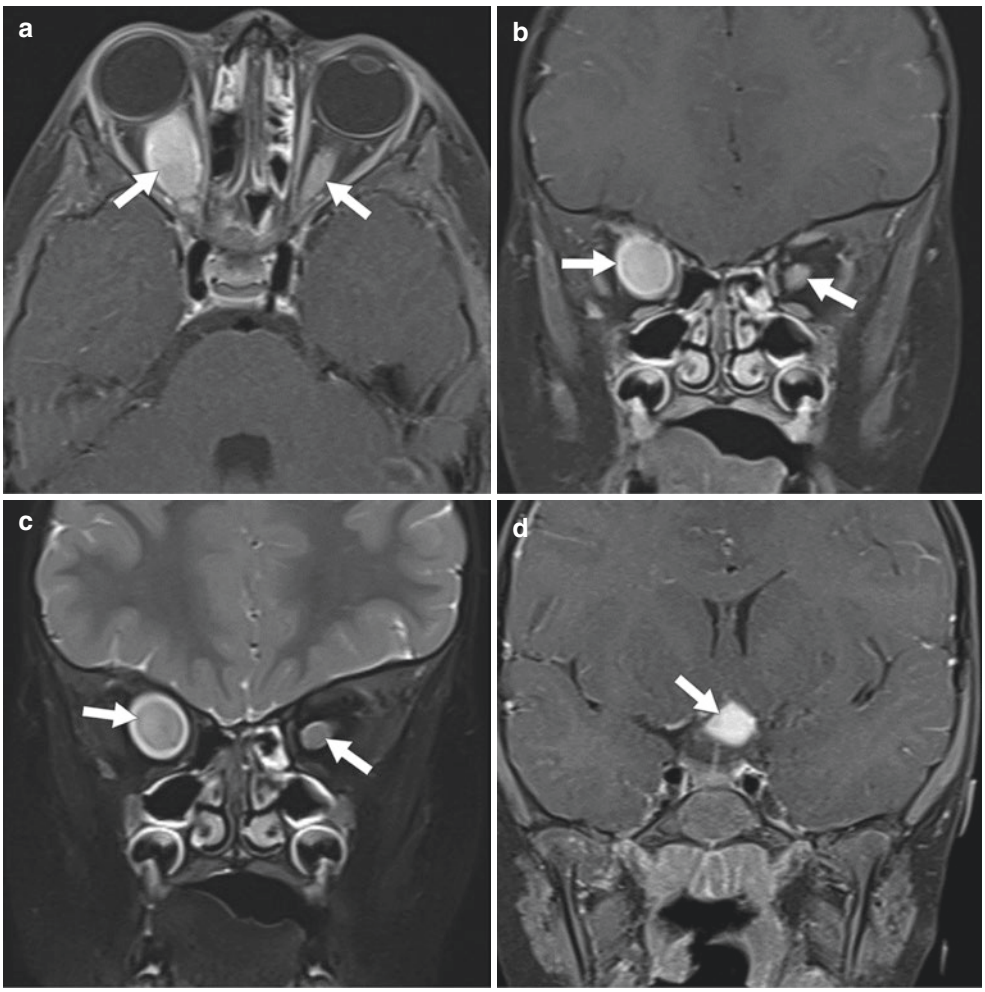

Fig. 10.10 A 3-year-old female with NF-1 and right eye vision loss. (**a**, **b**) Axial and coronal T1 post-contrast MRI with fat saturation show **homogeneously enhancing bilateral optic nerve gliomas** (arrows). (**c**) Coronal T2 MRI with fat saturation shows **iso- to hyperintense signal of the gliomas** (arrows). (**d**) Coronal T1 post-contrast MRI with fat saturation shows a **separate enhancing optic chiasm glioma** (arrow)

Background

- The majority are **pilocytic astrocytomas (WHO grade I)** [11].
- Usually associated with **NF-1** [11, 12].

Presentation

- Most common in **children (75%)**; no gender bias [11].
- **More aggressive in adults; in which case, there may be no association with NF-1** [12].
- Can be bilateral and multifocal if associated with NF-1.
- **Optic nerve** is the most common site in patients **with NF-1.**
- **Optic chiasm** is the most common site in patients **without NF-1** [13].
- **Symptoms**: decreased vision, proptosis [14, 15].

Imaging

- **Fusiform or exophytic optic nerve enlargement**.
- **Optic nerve may be elongated with kinking or buckling** [16].
- Absence of calcifications.
- **Most are lobulated solid tumors**.
  - **Cystic components** have been described, **particularly in patients without NF-1** [15].

CT

- **Isointense** to optic nerve with **homogeneous enhancement**.

MRI

- **T1 iso- to hypointense** to contralateral optic nerve with **variable enhancement**.
- **T2 iso- to hyperintense** [13, 15].

Key Points

- Review the orbital apex, optic nerve to the optic chiasm, hypothalamus, and the optic tracts.

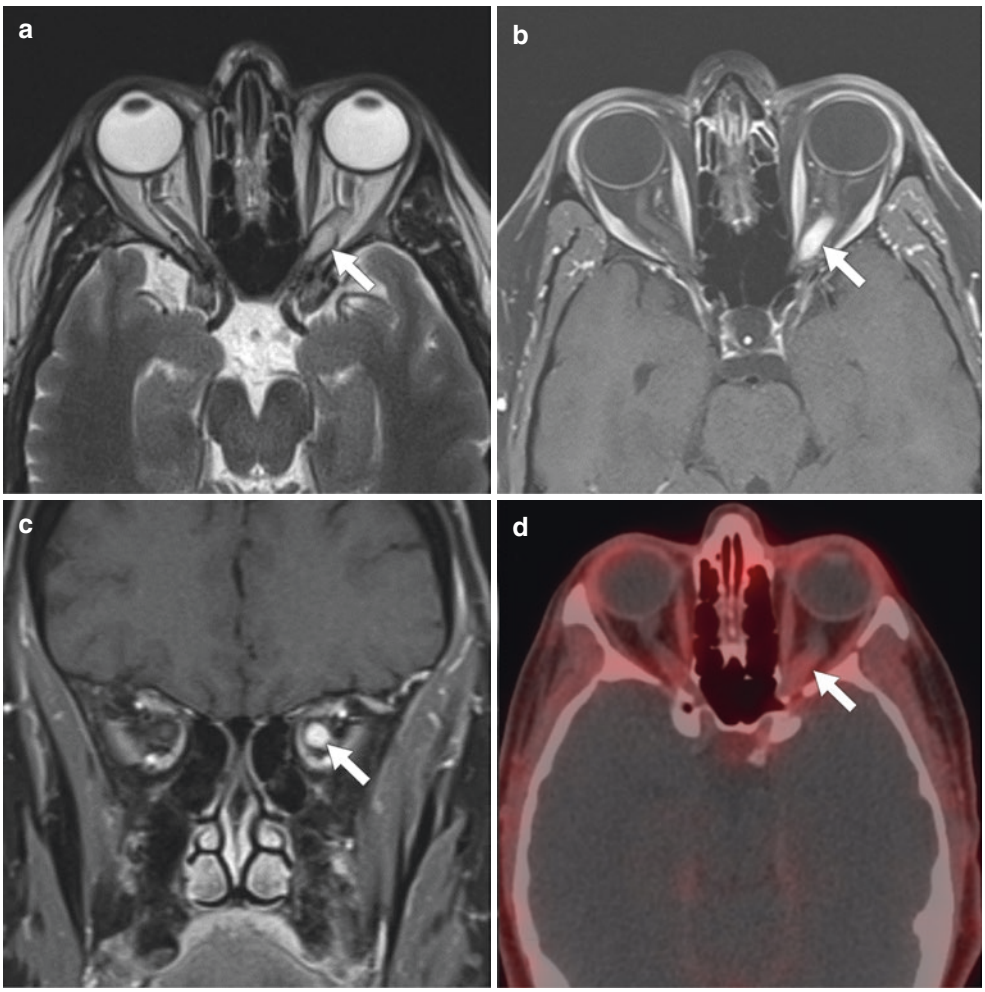

Fig. 10.11 A 51-year-old male with vision changes over the past 2 years. The patient was referred for a left optic nerve lesion with the differential diagnosis of glioma versus meningioma. (**a**) Axial T2 MRI with fat saturation shows **hyperintense signal in an expanded left optic nerve** (arrow). (**b**, **c**) Axial and coronal T1 post-contrast MRI with fat saturation shows **homogeneous, fusiform enhancement of the left optic nerve lesion** (arrows). (**d**) ^{68}Ga-DOTATATE PET/CT shows a **lack of avidity of the lesion** (arrow). The compilation of imaging findings is in keeping with an **optic nerve glioma**

Optic Neuritis

Figures 10.12 and 10.13 show cases of optic neuritis.

Background

- **Inflammatory process involving the optic nerve** [13].
- **Etiologies**: autoimmune diseases, e.g., multiple sclerosis, neuromyelitis optica; systemic diseases, e.g., system lupus erythematosus, sarcoidosis, Wegener disease, Sjogren's syndrome, and Behcet disease [17].

Presentation

- **Symptoms**: vision loss, painful eye movements [8].

Imaging

- **Optic nerve appears swollen** [8].
- **Fat stranding around the nerve from inflammation.**

MRI

- **T2 hyperintense**.
- **Enhances with contrast** [8].

Key Points

- Search for fat stranding.

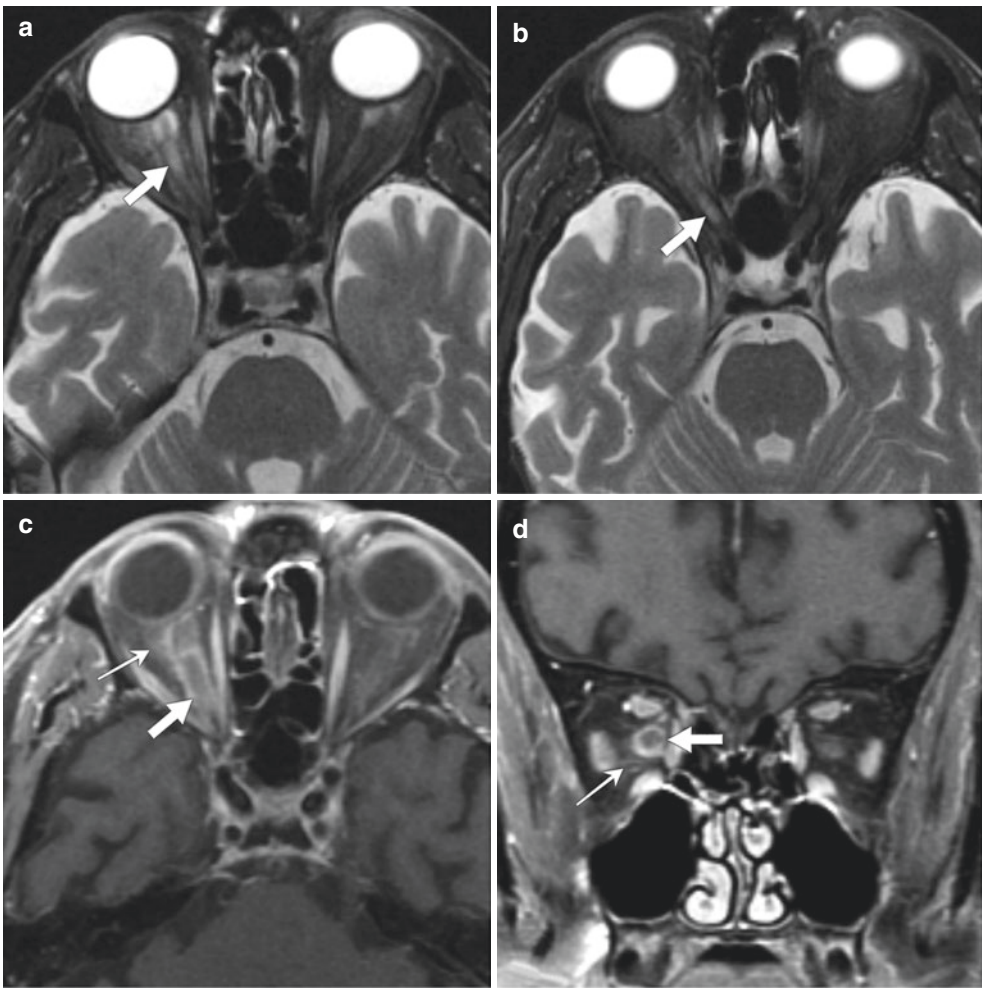

Fig. 10.12 A 79-year-old male with acute lymphoid leukemia and right eye blindness that was diagnosed as optic neuritis. (**a**, **b**) Axial T2 MRI with fat saturation shows **hyperintense signal in the intraorbital and canalicular segments of the right optic nerve** (arrows). (**c**, **d**) Axial and coronal T1 post-contrast MRI with fat saturation shows **enhancement of an enlarged right optic nerve and sheath** (arrows). Note **stranding in the adjacent intraconal fat** (thin arrows)

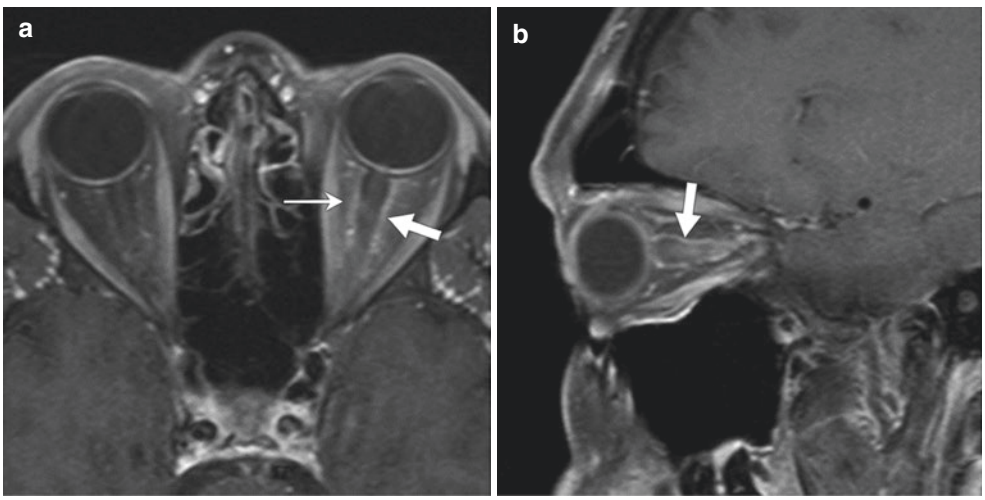

Fig. 10.13 A 57-year-old male with metastatic melanoma who presented with left ocular pain and optic nerve swelling noted on ophthalmologic examination and diagnosed as optic neuritis. (**a**–**c**) Axial, sagittal, and coronal T1 post-contrast MRI with fat saturation shows **enhancement of the left optic nerve and sheath** (arrows). Note **stranding in the adjacent intraconal fat** (thin arrows). (**d**) Coronal T2 MRI with fat saturation shows **signal hyperintensity in the swollen left optic nerve** (arrow)

Fig. 10.13 (continued)

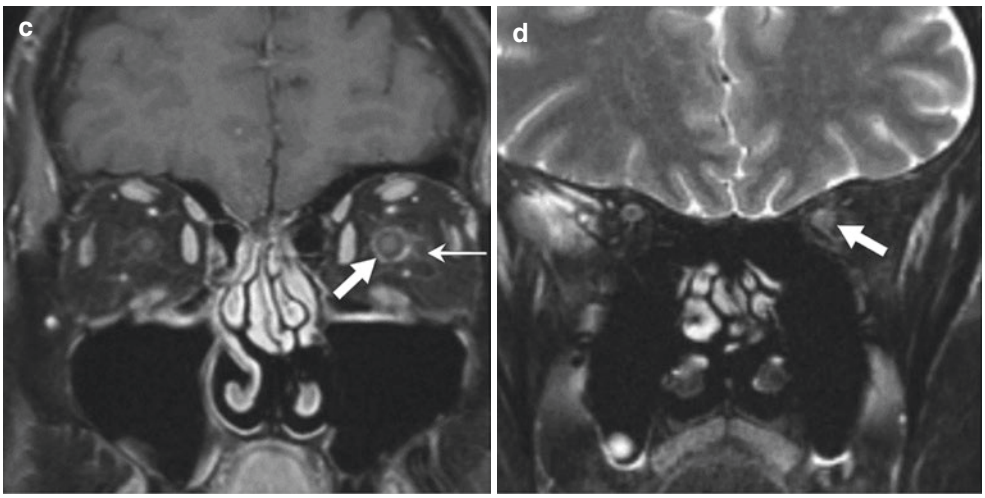

Nerve Sheath Tumors

Figures 10.14, 10.15, and 10.16 show cases of nerve sheath tumors.

Background

- Benign nerve sheath tumors are comprised of spindle cells arranged in **compact (Antoni type A)** or **loose (Antoni type B) tissues** [18].
- The **most involved nerves** about the orbit are the **trigeminal (CN V) and facial (CN VII) nerves**.
- **Soft tissue sarcomas** that originate from the peripheral nerve sheath are termed **malignant peripheral nerve sheath tumors (MPNSTs)** [19].
- **Intracranial schwannomas** may be associated with **NF-2**.
  - **Genetic condition with multiple schwannomas including bilateral vestibular schwannoma, meningiomas, and ependymomas** [20].
- **Neurofibromas** are typically associated with **NF-1**.
  - **Genetic condition of neurofibromas with iris hamartomas, optic nerve gliomas, osseous lesions, café au lait spots, and axillary or inguinal freckling**.
  - Can show malignant transformation.
  - **Rarely involve the cranial nerves** [21].

Presentation

- **Denervation atrophy of innervated muscle or a sensory deficit** can aid in **identifying** the **nerve of origin or an adjacent cranial nerve** from long-standing mass effect [20].

Imaging

- **Slow growth** characterized by **smooth expansion of an affected neural foramen, bone remodeling, and/or mass effect on adjacent soft tissues** [20, 22].
- **Clinical symptoms suggesting transformation to an MPNST**: nonspecific and include new pain, increased growth, and new neurologic deficits [23].

CT

- **Hypo- to isodense** [20].
- Cranial nerve schwannomas demonstrate **variable enhancement** [22, 24].

MRI

- **Appearance depends on the components of Antoni type A and B tissues** [18].
- **T1 hypo- to isointense with avid enhancement**.
- **T2 heterogeneously hyperintense** due to compactly arranged cells (Antoni type A pattern - hypointense) intermixed with areas of loosely arranged cells (Antoni type B pattern - hyperintense) with variable water content and cellularity [18, 25]. Therefore, nerve sheath tumors **can be hypo- to isointense** [26].
- **Larger lesions may demonstrate heterogeneous enhancement, internal cysts, and hypointense foci of hemosiderin related to internal hemorrhage** [20].
- **MRI findings of MPNSTs**: interval growth, larger size, heterogeneous signal and enhancement, internal necrosis without enhancement, irregular margins, and local invasion [26].
- **Restricted diffusion associated with MPNSTs** has been described [26]; however, further work on this topic is needed [19].

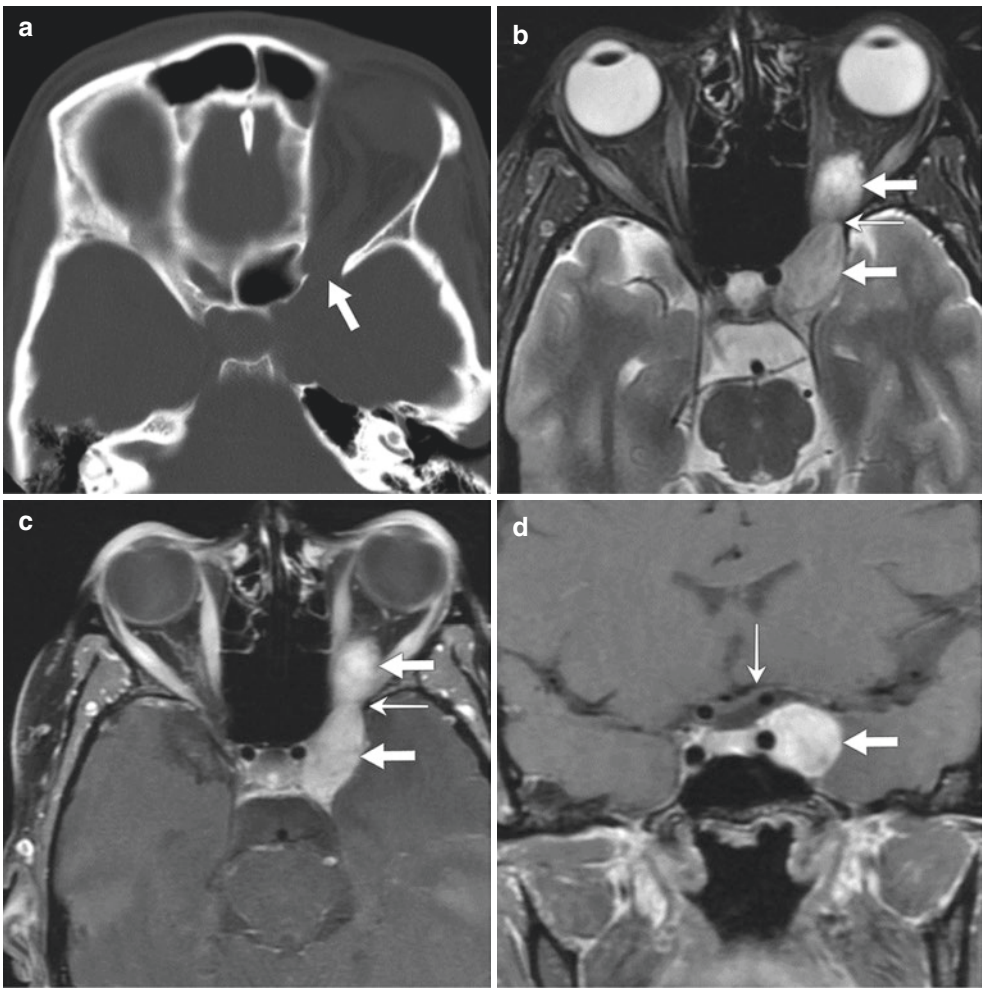

Fig. 10.14 A 34-year-old female with an incidentally discovered left orbital schwannoma. (**a**) Axial CT without contrast, bone window shows **widening of the left superior orbital fissure** (arrow). (**b**) Axial T2 MRI with fat saturation shows an **iso- to hyperintense appearance of a left posterior orbit and cavernous sinus schwannoma** (arrows). Note the **narrowing of the schwannoma as it passes through the superior orbital fissure** (thin arrow). (**c**) Axial T1 post-contrast MRI with fat saturation shows **homogeneous enhancement of the schwannoma** (arrows) with **narrowing as it passes through the superior orbital fissure** (thin arrow). (**d**) Coronal T1 post-contrast MRI with fat saturation shows **homogeneous enhancement of the cavernous sinus component** (arrow) with **elevation of the left side of the optic chiasm** due to local mass effect (thin arrow)

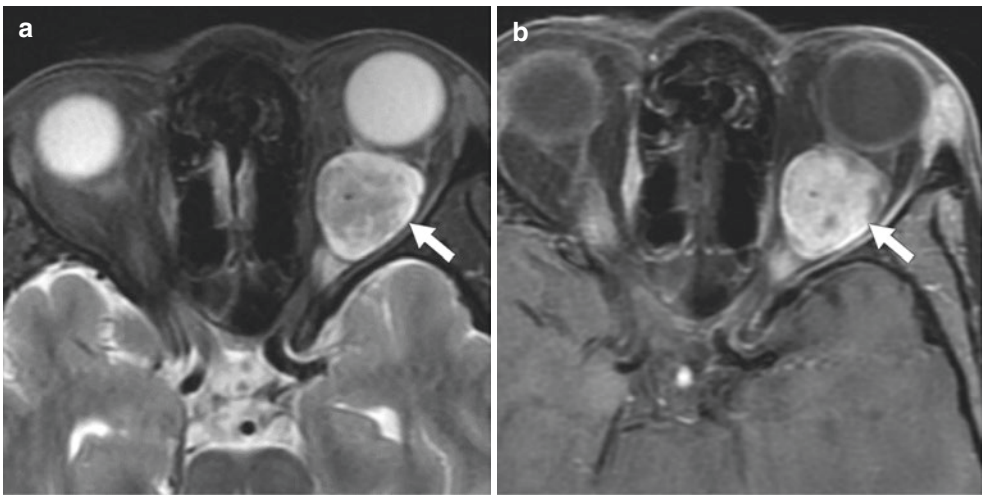

Fig. 10.15 A 46-year-old female with left proptosis and a left orbital mass detected on imaging. Subsequent resection revealed a schwannoma. (**a**) Axial T2 MRI with fat saturation shows a **well-circumscribed iso- to hyperintense mass in the left orbit** (arrow). (**b–d**) Axial, coronal, and sagittal T1 post-contrast MRIs with fat saturation show **fairly homogeneous enhancement of the schwannoma** (arrows)

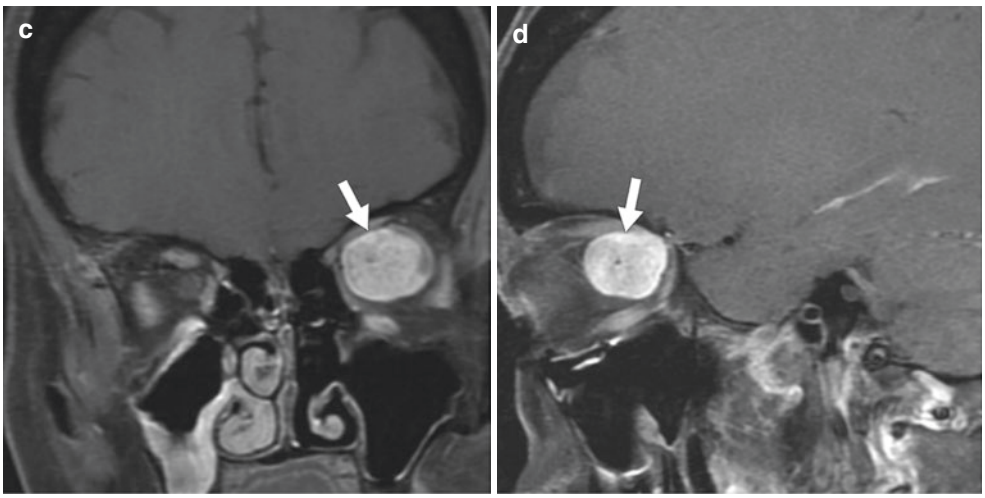

Fig. 10.15 (continued)

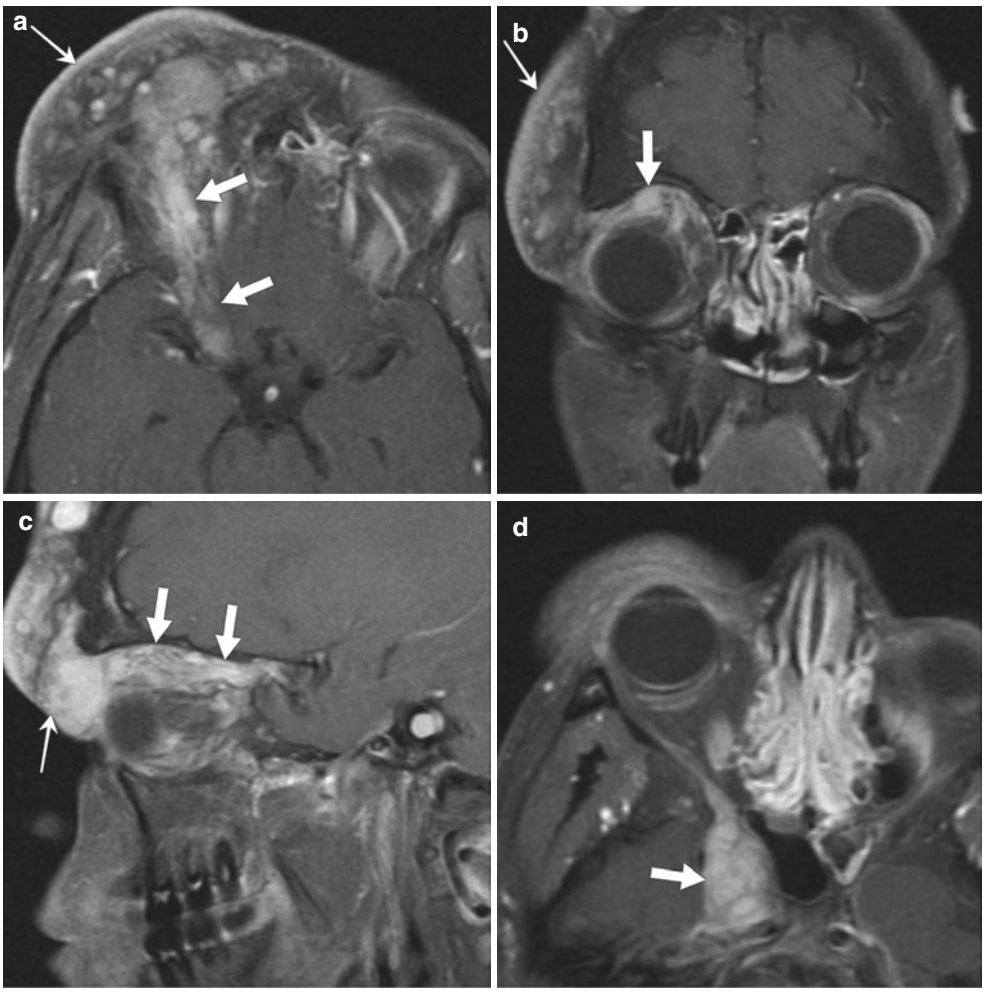

Fig. 10.16 A 20-year-old male with NF-2 and a right facial plexiform neurofibroma. (**a**–**c**) Axial, coronal, and sagittal T1 post-contrast MRI with fat saturation shows **heterogeneous enhancement of the right frontal scalp and face plexiform neurofibroma** (thin arrows). There is **extension along the ophthalmic division of the right trigeminal nerve (V_1)** (arrows) **through the superior orbital fissure**. (**d**) Axial T1 post-contrast MRI with fat saturation shows **further posterior extension of the neurofibroma to involve the right cavernous sinus** (arrow)

PET

- In addition to **intense ^{18}F-FDG avidity,** both schwannomas and MPNSTs may be large and demonstrate a heterogeneous appearance [26].

Key Points

- **Review the cranial nerve to detect all lesions**.
- Search for signs to suggest **transformation to a MPNST**.

Perineural Tumor Spread

Figures 10.17, 10.18, and 10.19 show cases of perineural tumor spread.

Background

- **Microscopic spread of tumor along the nerve sheaths** [27].
- **May extend a substantial distance** from the primary tumor [28].
- **Disruption of the blood-nerve barrier** results in increased endoneural capillary permeability allowing for the **leakage and accumulation of contrast material leading to enhancement of the nerve** [29].
- **Most common tumors**: **adenoid cystic and squamous cell carcinoma**. It can also occur with basal cell carcinoma, lymphoma, melanoma, melanoma, rhabdomyosarcoma, and juvenile angiofibroma [21].
- Associated with **decreased overall survival** [30].

Presentation

- **Symptoms**: pain, dysesthesias (abnormal sensations such as painful burning, itching, stinging), or denervation atrophy of innervated muscle [21].
- **Most affected nerves**: maxillary (V_2) and mandibular (V_3) divisions of the trigeminal nerve and the facial nerve [21].

Imaging

- **Signs of perineural tumor involvement: nerve enlargement with enhancement**; **replacement of neuroforaminal fat**, **enlargement or destruction of the foramen, denervation atrophy of innervated muscle** [28].
- An affected nerve can **maintain its normal size while passing through the skull base foramina**.
- **Neuritis from chemoradiation** may occur months to years after treatment and **may be difficult to distinguish from perineural tumor spread** [30, 31].

MRI

- **Invasion of the skull base** may present as **the replacement of normal fatty marrow signal** [21].
- **Denervated muscles** have characteristic MRI patterns [32].
  - **Acute** (<1 month): **T2 hyperintensity, enhancement, and increased volume**.
  - **Subacute** (up to 12–20 months): **T1 hyperintensity due to fat deposition without volume loss**.
  - **Chronic** (>12–20 months): **Fatty atrophy with volume loss**.

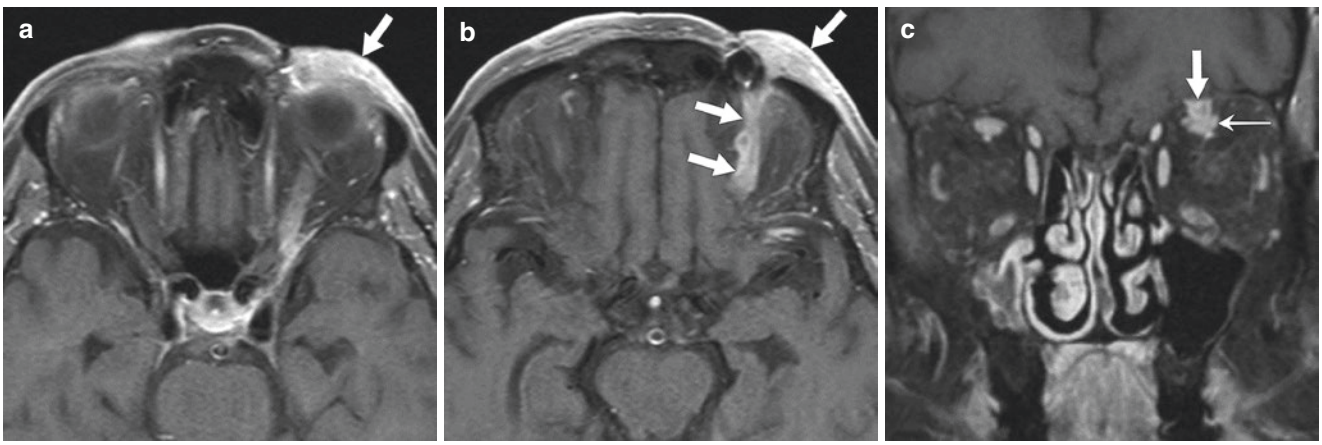

Fig. 10.17 A 77-year-old male with left forehead squamous cell carcinoma who presented with ptosis (drooping eyelid) and diplopia on superior gaze. (**a**) Axial T1 post-contrast MRI with fat saturation shows an **enhancing mass in the left upper eyelid** (arrow). (**b**) Axial T1 post-contrast MRI with fat saturation shows the **enhancing left forehead mass with perineural spread along the ophthalmic division of the left trigeminal nerve (V_1)** (arrows). (**c**) Coronal T1 post-contrast MRI with fat saturation shows **perineural spread along the left V_1 nerve** (arrow). The enhancement is **inseparable from the adjacent superior rectus-levator complex** (thin arrow), which is likely involved, given the clinical history of diplopia on superior gaze

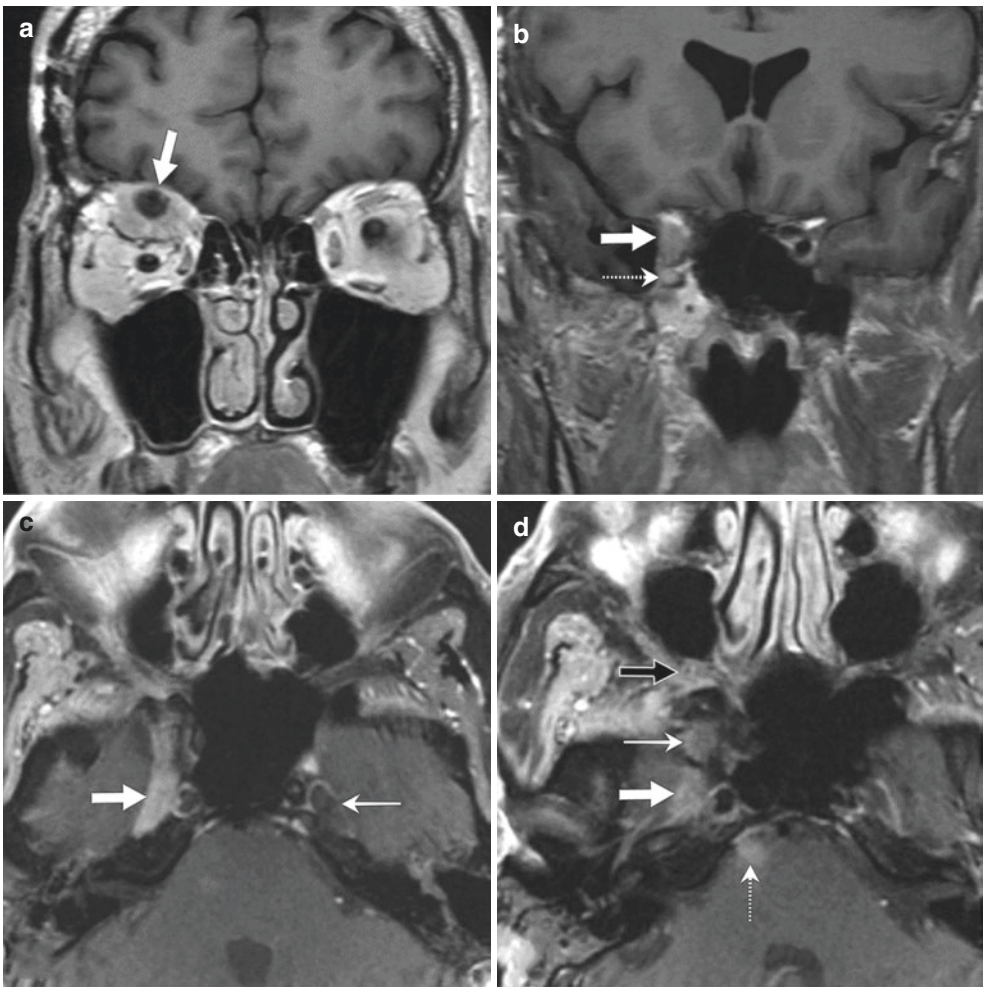

Fig. 10.18 A 51-year-old male with squamous cell carcinoma of the skin of the face presented with right proptosis. (**a**) Coronal T1 post-contrast MRI without fat saturation shows **perineural tumor along the ophthalmic division of the right trigeminal nerve (V_1)** (arrow) that is **indistinguishable from the superior rectus-levator complex**. (**b**) Coronal T1 post-contrast MRI with fat saturation shows **perineural spread to the right cavernous sinus** (arrow) and **involvement of the right maxillary division of the right trigeminal nerve (V_2) in the foramen rotundum** (thin arrow). (**c**) Axial T1 post-contrast MRI with fat saturation shows **disease spread to the right Meckel's cave** (arrow). Note the normal appearance of the left Meckel's cave (thin arrow). (**d**) Axial T1 post-contrast MRI with fat saturation shows **perineural spread of disease in the right Meckel's cave** (white arrow), **along the mandibular division of the right trigeminal nerve (V_3)** (thin white arrow), and **in the right pterygopalatine fossa** (black arrow). **Enhancement is also present in the anterior pons** (dotted white arrow), **presumably related to perineural spread along the right abducens nerve from the cavernous sinus**

Key Points

- **MRI with fat suppression** can aid in visualization.
- Comment on the **number of lesions** and **other sites** of involvement.
- Evaluate the entire nerve to assess for **skip lesions**.
- **Differentiate** between extension from the **primary tumo**r versus a **separate metastasis**.
- In selected cases, abnormal soft tissue adjacent to cranial nerves can be sampled with image-guided fine-needle aspiration [33].
- **Nerve enhancement may persist indefinitely even if there is clinical evidence of improvement. Radiographic and clinical progression are important indicators of recurrent tumor** [34].

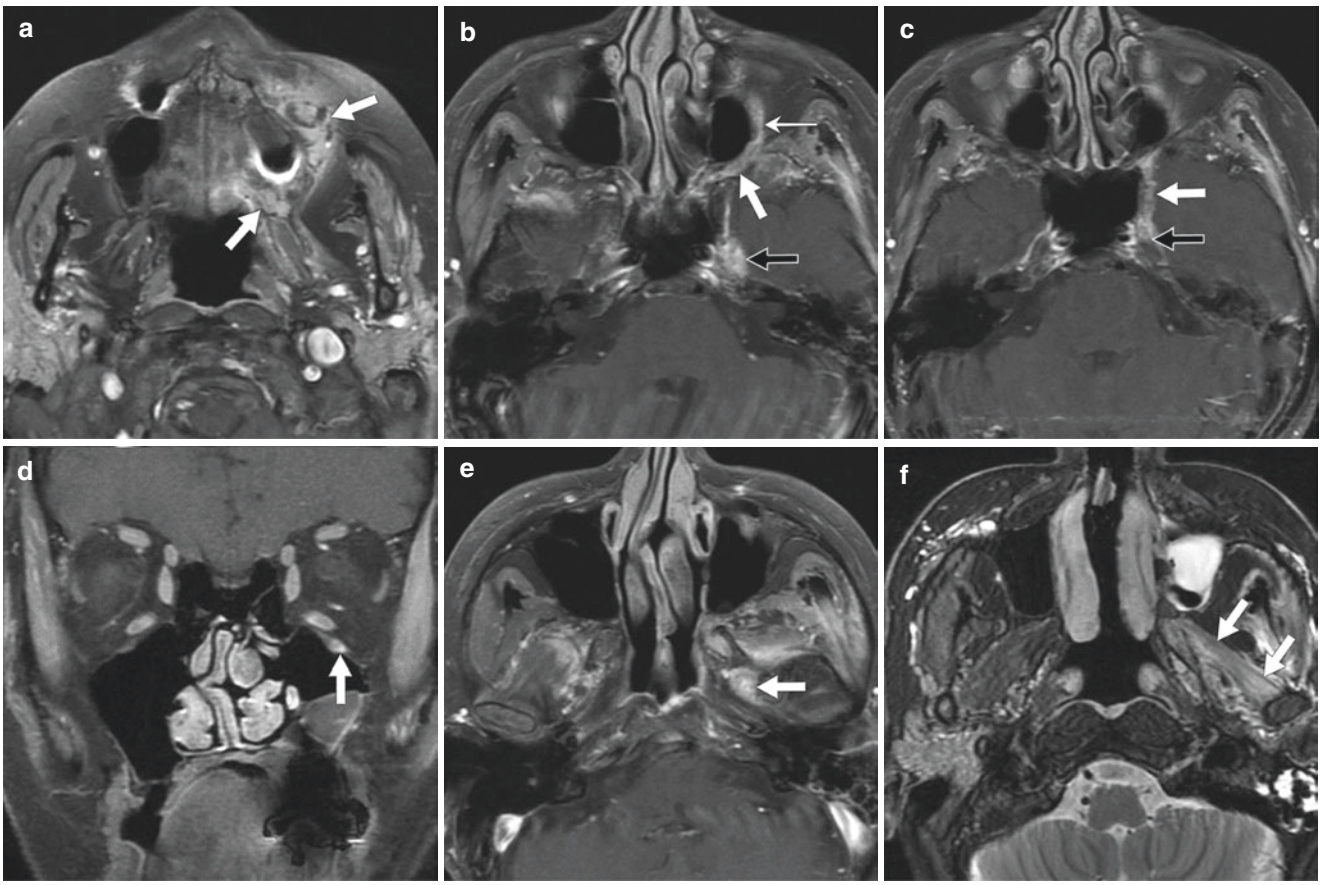

Fig. 10.19 An 85-year-old female with hard palate adenoid cystic carcinoma and facial numbness to the V_2 and V_3 areas. (**a**) Axial T1 post-contrast MRI with fat saturation shows **enhancement of the left hard palate and buccal space** (arrows). (**b**) Axial T1 post-contrast MRI with fat saturation shows **perineural spread to the left pterygopalatine fossa** (white arrow) via the palatine nerves. **Further perineural spread is also seen through the inferior orbital fissure and along the infraorbital nerve (V_2)** (thin white arrow). **Perineural tumor spread through the foramen rotundum and the cavernous sinus to the left Meckel's cave** (black arrow). (**c**) Axial T1 post-contrast MRI with fat saturation shows **perineural spread along the left V_2 nerve in the foramen rotundum and cavernous sinus (white arrow) and involving the anterior left Meckel's cave** (black arrow). (**d**) Coronal T1 post-contrast MRI with fat saturation shows **perineural spread to the left infraorbital nerve (V_2)** (arrow). (**e**) Axial T1 post-contrast MRI with fat saturation shows **perineural spread along the mandibular division of the left trigeminal nerve (V_3) in the foramen ovale** (arrow). (**f**) Axial T2 MRI with fat saturation shows **denervation atrophy of the left muscles of mastication** (arrow)

Leptomeningeal Disease

Figures 10.20, 10.21, 10.22, and 10.23 show cases of leptomeningeal disease.

Background

- Leptomeningeal disease (LMD) is a **complication of late-stage systemic cancers**.
  - **Infiltration of the leptomeninges by tumor cells** [35].
- **Both primary and secondary tumors** can spread through the subarachnoid spaces and along cranial nerves.
  - **Primary tumors**: medulloblastoma, oligodendroglioma ependymoma, and glioblastoma.
  - **Secondary tumors**: breast and lung cancer and melanoma.
- **CN VII and VIII are the most affected cranial nerves** [35].
- **Neurolymphomatosis**: term used when hematologic malignancies such as lymphoma spread along cranial and peripheral nerves [36].
  - Most often encountered with **diffuse large B cell lymphoma**.
  - **Can occur months to years after the original diagnosis**.

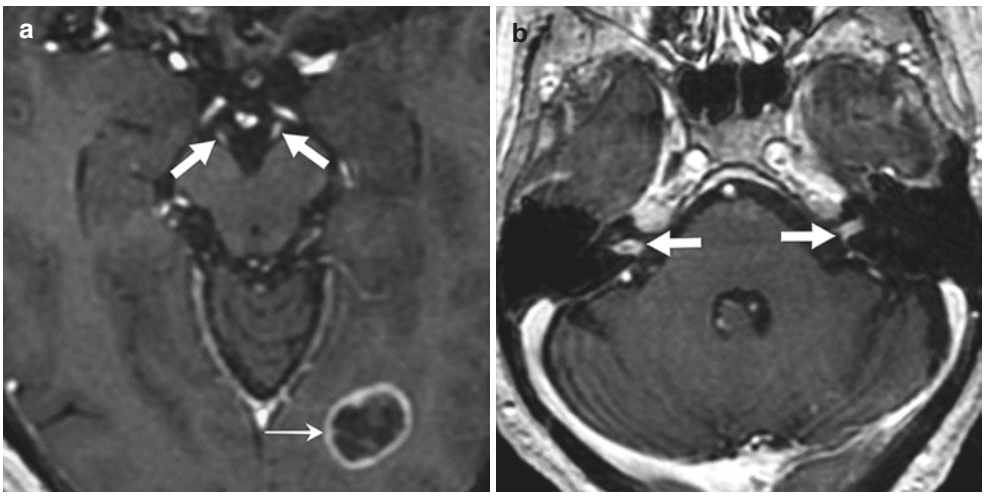

Fig. 10.20 A 74-year-old female with breast cancer who presented with headaches. (**a**) Axial T1 post-contrast MRI with fat saturation shows a **left occipital lobe metastasis** (thin arrow). **Enhancement of the oculomotor nerves from leptomeningeal tumor spread** (arrows). (**b**) Axial T1 post-contrast MRI with fat saturation shows **LMD in the internal auditory canals along the bilateral seventh/eighth cranial nerve complexes** (arrows)

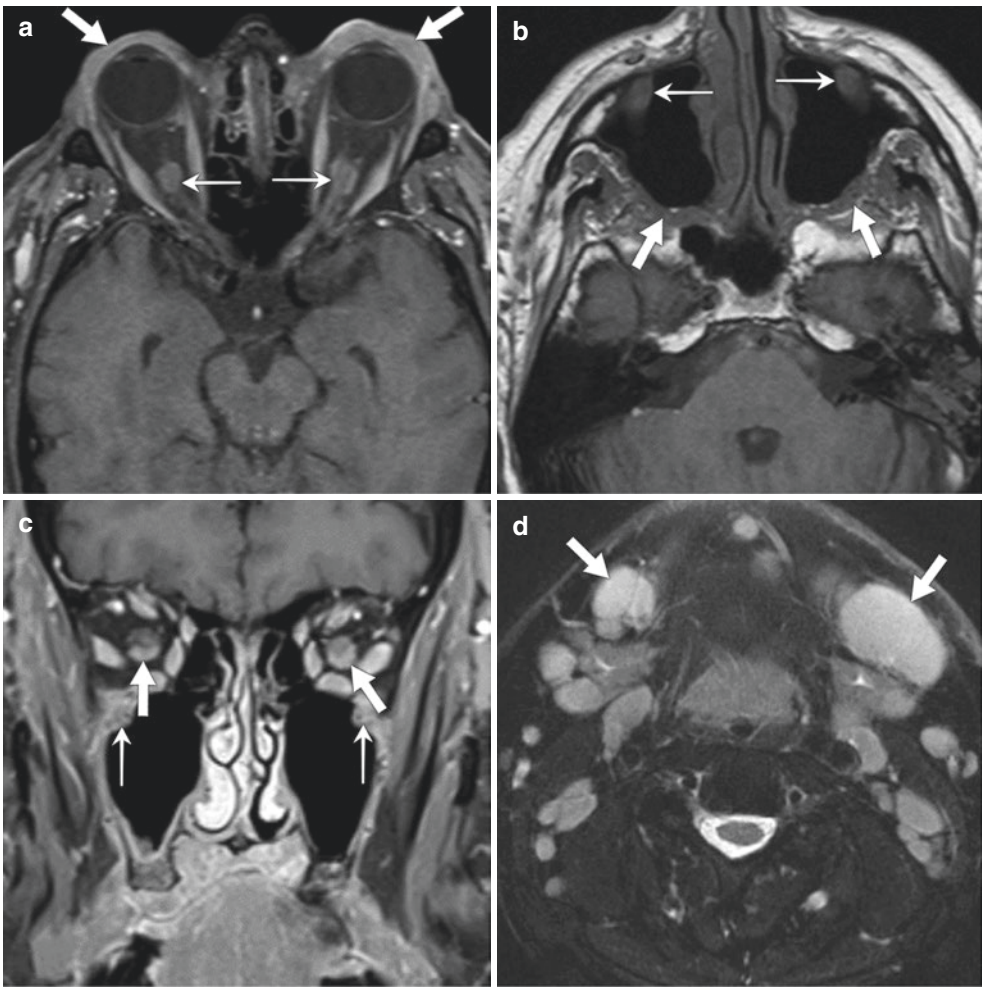

Fig. 10.21 A 70-year-old male with mantle cell lymphoma who presented with "lumps" on his eyelids. (**a**) Axial T1 post-contrast MRI with fat saturation shows **enhancing lesions in bilateral eyelids** (arrows). **Enhancing soft tissue is also present around bilateral optic nerves** (thin arrows). (**b**) Axial T1 non-contrast MRI without fat saturation shows **soft tissue filling the pterygopalatine fossae with replacement of normal fat** (arrows) **and involving enlarged infraorbital nerves** (thin arrows). (**c**) Coronal T1 post-contrast MRI with fat saturation shows **enhancement around the optic nerves** (arrows) **and involving the infraorbital nerves (V_2)**. (**d**) Axial T2 MRI with fat saturation shows **multiple enlarged neck nodes** (arrows)

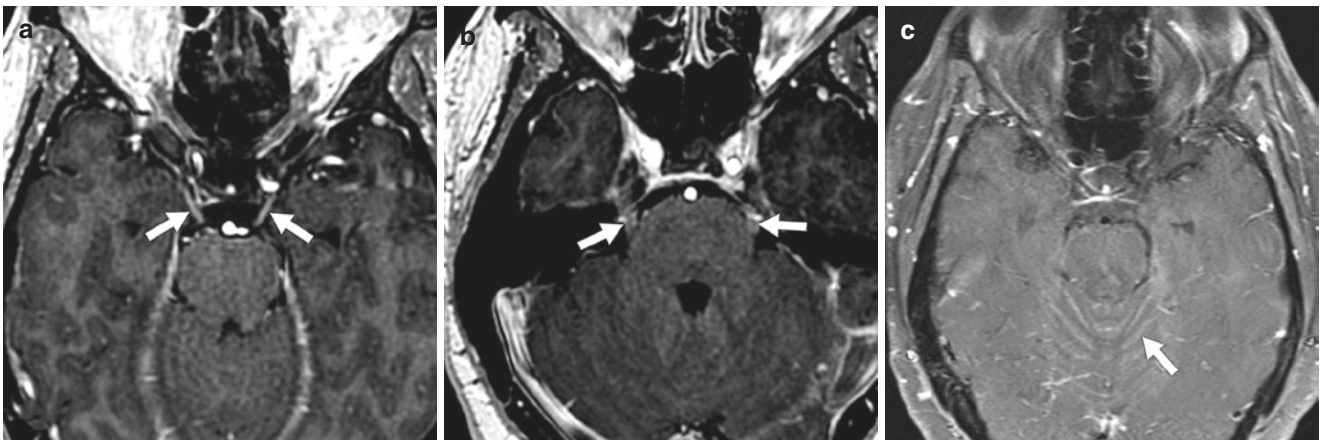

Fig. 10.22 A 32-year-old male with acute myeloid leukemia who presented with facial pain due to neurolymphomatosis. (**a**) Axial T1 post-contrast MRI without fat saturation shows **enhancement of the oculomotor nerves** (arrows). (**b**) Axial T1 post-contrast MRI without fat saturation shows **enhancement of the trigeminal nerve roots** (arrows). (**c**) Axial T1 post-contrast MRI with fat saturation shows **enhancing LMD in the cerebellar folia** (arrow)

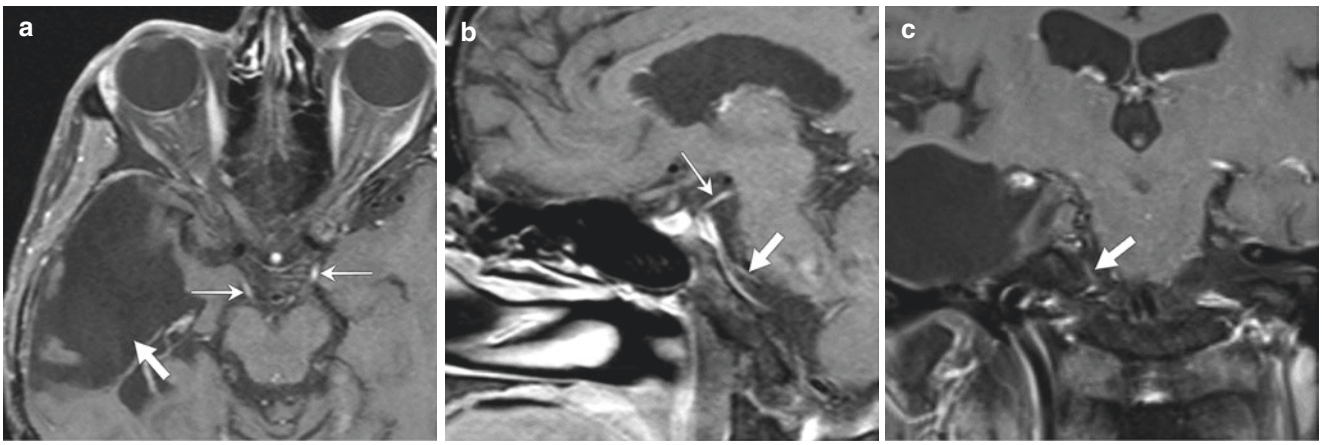

Fig. 10.23 A 54-year-old male after resection of a right temporal glioblastoma who presented with diplopia. Physical examination revealed right oculomotor (CN III) and abducens (CN VI) nerve palsies. (**a**) Axial T1 post-contrast MRI with fat saturation shows a **postoperative cavity following resection of the right temporal lobe glioblastoma** (arrow) and **enhancement of bilateral oculomotor nerves** (thin arrows). (**b**) Sagittal T1 post-contrast MRI with fat saturation shows **enhancement of the right oculomotor** (thin arrow) **and abducens** (arrow) **nerves**. (**c**) Coronal T1 post-contrast MRI with fat saturation shows **enhancement of the right abducens nerve** (arrow). The patient's physical examination and MRI findings have remained stable for over a year. Clinically, the cranial nerve enhancement was felt to be related to prior radiation treatment

Presentation

- **Symptoms**: cranial neuropathies, mental status changes [35, 36].
- **Ocular disturbance** (cranial nerve deficits, optic disc or retinal infiltration, papilledema) reported in 67% of patients with LMD [37].

Imaging

- **Nerves are enlarged and enhanced** [35].
- Neurolymphomatosis of the orbital cranial nerves most commonly occurs via direct spread from a solid mass in the orbit or maxillofacial region [36].

Key Points

- **Lack of detection can lead to delayed diagnosis** [38].
- **MRI with fat suppression** can aid in visualization.
- **T1 non-contrast-enhanced MRI** can sometimes better detect disease in the pterygopalatine fossae, characterized by fat replacement.

- Comment on the **number of lesions** and **other sites** of involvement.
- Evaluate the entire nerve to assess for **skip lesions**.

Idiopathic Orbital Inflammation (IOI)

Figures 10.24 and 10.25 show cases of idiopathic orbital inflammation.

Background

- Idiopathic orbital inflammation (IOI) was previously referred to as orbital pseudotumor.
- IOI is an **inflammatory condition characterized by polymorphous infiltration and variable degrees of fibrosis** [39, 40].
- After thyroid orbitopathy and lymphoproliferative disorders, IOI is the **third most common disease to affect the orbit** [41].

Presentation

- **Symptoms**: proptosis, headache, **periorbital pain**, and inflammatory signs, e.g., swelling and erythema.
- **Compression upon the orbital apex and cavernous sinus involvement may lead to decreased visual acuity** and **cranial nerve palsies** [42].

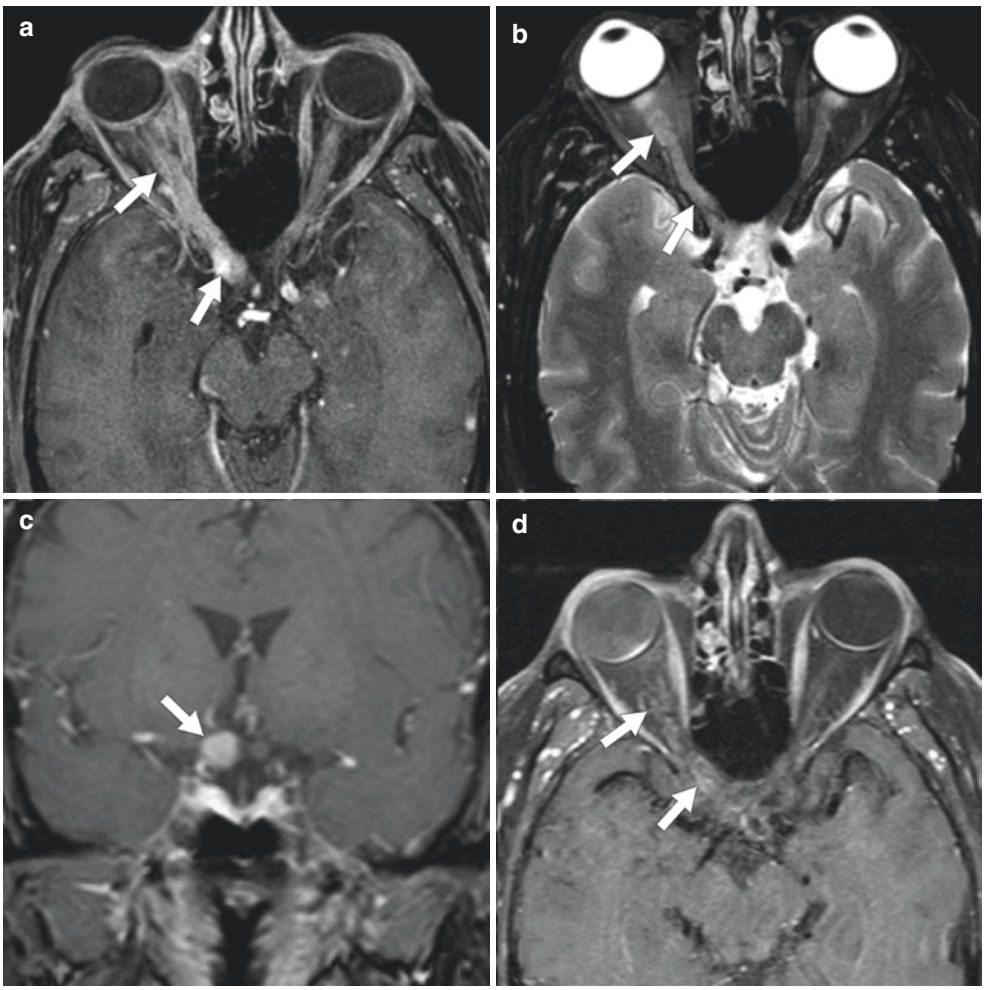

Fig. 10.24 A 54-year-old male had decreased vision in the right eye due to IOI. (**a**) Axial T1 post-contrast MRI with fat saturation shows **an enlarged enhancing right optic nerve** (arrow) and **intraconal space enhancement**. (**b**) Axial T2 MRI with fat saturation shows a **hyperintense appearance of the right optic nerve** (arrow). (**c**) Coronal T1 post-contrast MRI with fat saturation shows the **enhancing mass involving the prechiasmatic right optic nerve** (arrow). (**d**) Axial T1 post-contrast MRI with fat saturation shows the **decrease in size and degree of enhancement of the right optic nerve following steroid treatment** (arrows)

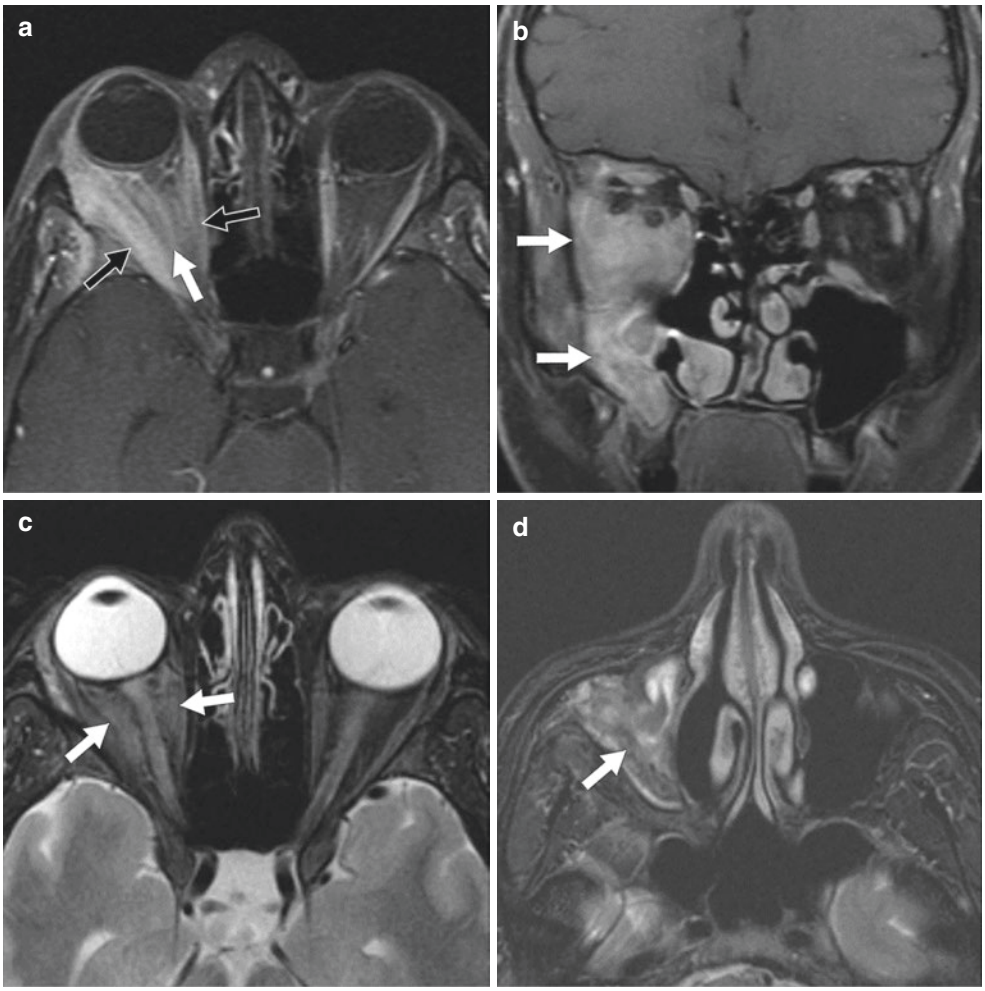

Fig. 10.25 An 18-year-old female with right conjunctival redness and periorbital pain due to biopsy-proven IOI. (**a**) Axial T1 post-contrast MRI with fat saturation shows **infiltrative tissue in the intraconal space of the right orbit** (white arrow) **and enlargement of the medial and lateral rectus muscles** (black arrows). (**b**) Coronal T1 post-contrast MRI with fat saturation shows **contiguous soft tissue in the right orbit and maxillary sinus** (arrows). (**c**, **d**) Axial T2 MRI with fat saturation shows an **iso- to hypointense appearance of the disease on the right orbit and maxillary sinus** (arrows)

Imaging

- **Retro-orbital involvement** may occur from spread through the superior and inferior orbital fissures and the optic canal, extending to the cavernous sinus.
- **Other sites of involvement**: optic nerve, including the junction with the globe, lacrimal gland, and adjacent peri-orbital soft tissues.
- When the **extraocular muscles** are involved, **IOI can include the tendinous portion of the muscles** [29].

CT

- **Enhancement with contrast** has been reported [42].

MRI

- **T1 isointense and T2 hypointense due to fibrosis**.
- **Variable contrast enhancement** [42].

Key Points

- Assess for cranial nerve and cavernous sinus involvement.
- **Describe involvement** and **signs of compression at the orbital apex**.

IgG4-Related Disease

Figures 10.26 and 10.27 show cases of IgG4-related disease.

Background

- Immunoglobulin G4-related disease (IgG4-RD) is a **systemic disease of unknown etiology.**
- Characterized by tissue **infiltration with plasma cells that express IgG4, inflammation, and fibrosis**.
- **Various organs may be involved,** including the pancreas, bile duct, liver, retroperitoneal soft tissues, lung,

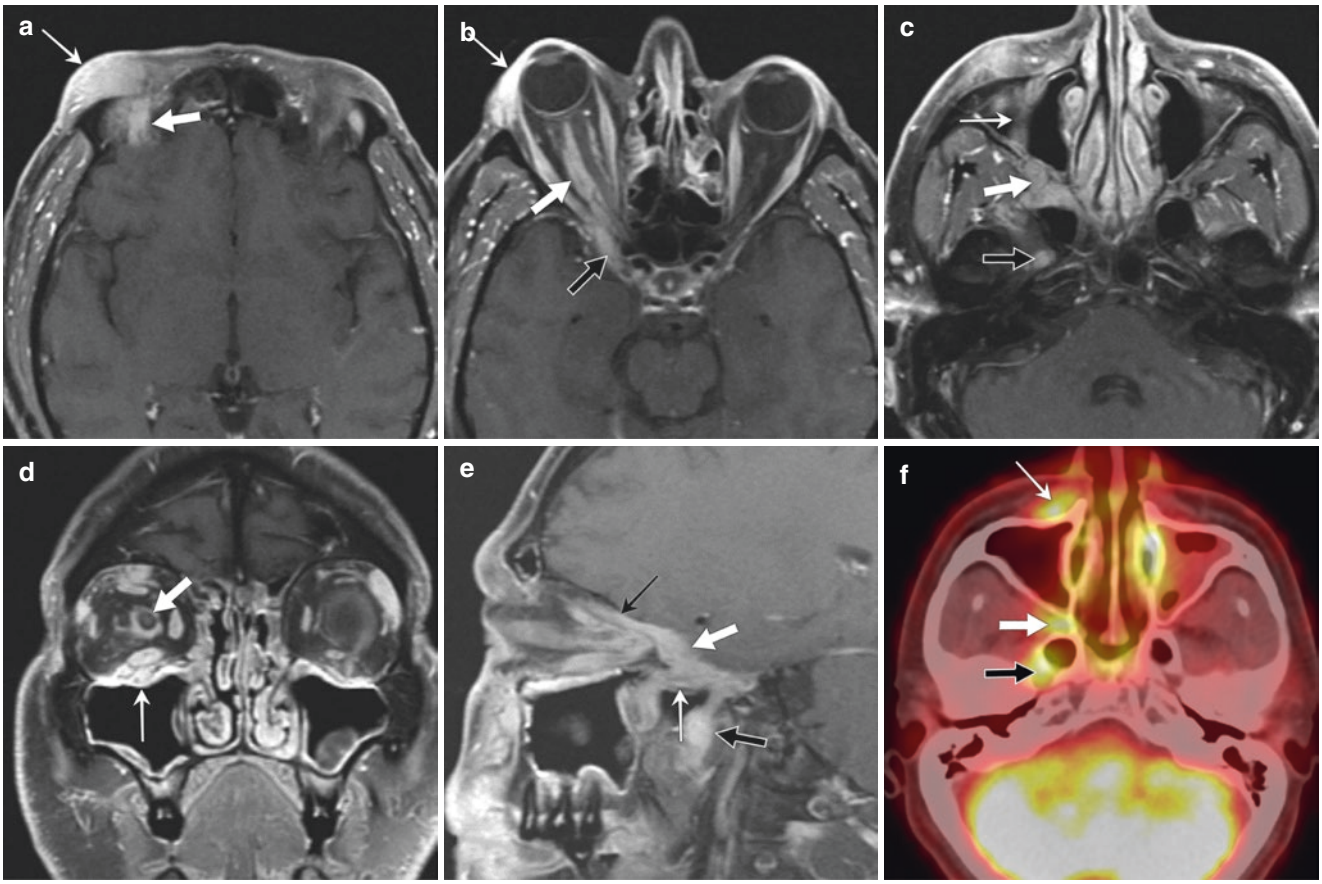

Fig. 10.26 A 43-year-old male with right orbital swelling due to IgG4-RD. (**a**) Axial T1 post-contrast MRI with fat saturation shows **enhancing tissue in the right forehead** (thin arrow) with **spread of disease along the right ophthalmic (V_1) nerve** (arrow). (**b**) Axial T1 post-contrast MRI with fat saturation shows **enhancing soft tissue in the eyelids and periorbital soft tissues** (thin arrow). **Enhancing soft tissue is present in the right intraconal space** (white arrow) and **extends through the superior orbital fissure to the cavernous sinus** (black arrow) (**c**) Axial T1 post-contrast MRI with fat saturation shows **enhancing soft tissue in the right pterygopalatine fossa** (white arrow) with **involvement of the right infraorbital nerve (V_2)** (thin white arrow), and the **mandibular nerve (V_3)** (black arrow). (**d**) Coronal T1 post-contrast MRI with fat saturation shows **enhancing tissue surrounding the right optic nerve** (arrow) and involving the **right infraorbital nerve (V_2)** (thin arrow). (**e**) Sagittal T1 post-contrast MRI with fat saturation shows enhancing disease involving the **ophthalmic (V_1)** (white arrow), **maxillary (V_2)** (thin white arrow), **and mandibular (V_3)** (black arrow) **divisions of the trigeminal nerve**. Note involvement of the **ophthalmic (V_1) nerve** (thin black arrow). (**f**) Axial ^{18}F-FDG PET/CT shows **FDG-avid lesions in the right premaxillary soft tissues** (thin white arrow), **right pterygopalatine fossa** (white arrow), **and the right maxillary nerve (V_3)** (black arrow)

thyroid, salivary glands, and lymph nodes, **either alone or systematically** [43, 44].

- **The head and neck is the second most affected site after the pancreas** [45].

Presentation

- Occurs primarily in **older men.**
- Often with **elevated serum IgG4 levels** [46].
- **Symptoms**: hypophysitis, thyroiditis, pancreatitis, cholecystitis, retroperitoneal fibrosis, and lymphadenopathy [45–48].

Imaging

- **Cavernous sinus disease often accompanies orbital and dural involvement**.
- The nerves appear thickened with enhancement when the cavernous sinus is involved [49].

CT

- **Soft tissue density of the disease**.

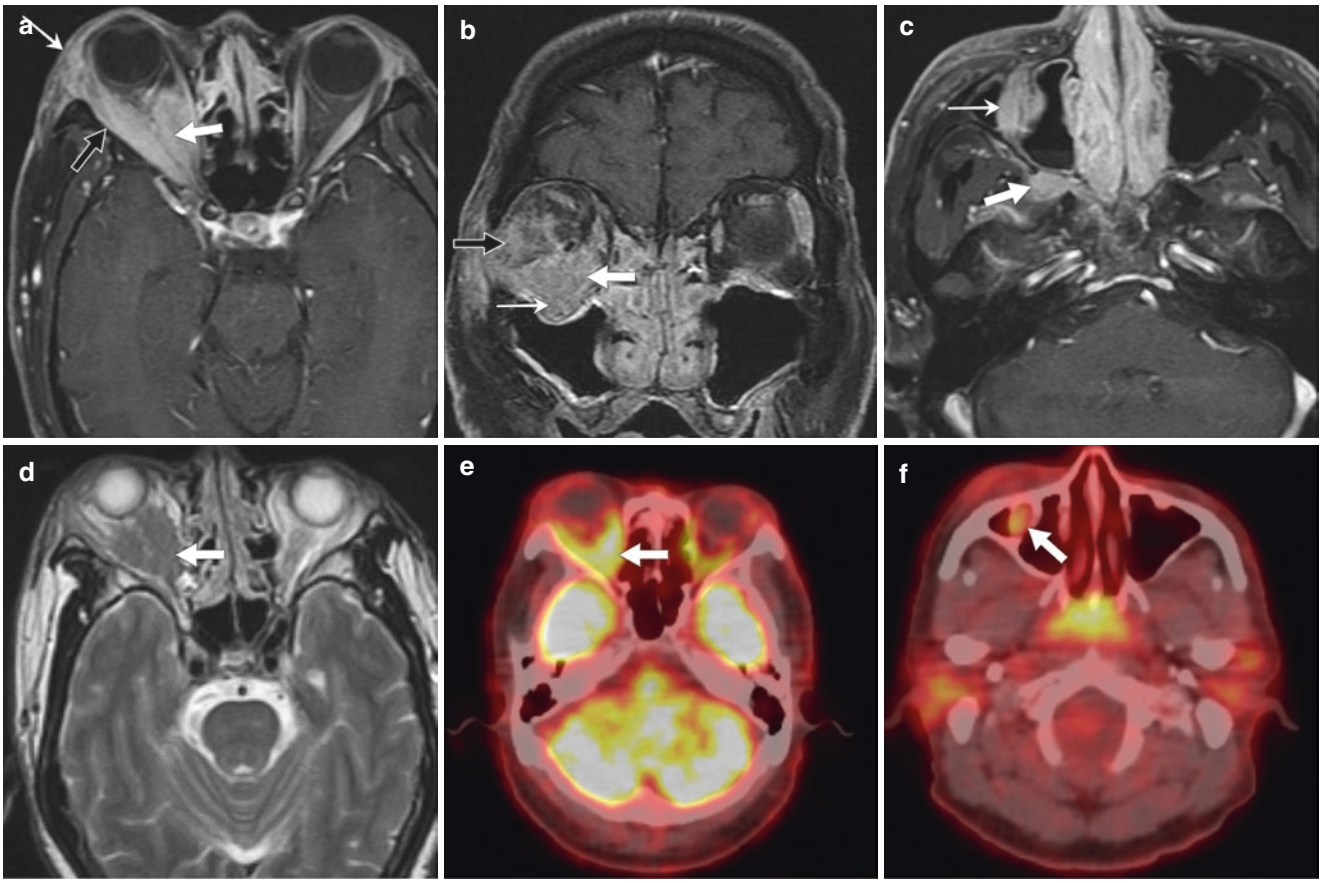

Fig. 10.27 A 60-year-old male with slowly progressive right proptosis for 6 months. (**a**) Axial T1 post-contrast MRI with fat saturation shows **proptosis with enhancing tissue in the right intraconal space** (white arrow) **with infiltration of the right lateral rectus muscle** (black arrow) **and periorbital soft tissues** (thin white arrow). (**b**) Coronal T1 post-contrast MRI with fat saturation shows **enhancing tissue in the right intraconal space** (white arrow) **with infiltration of the right lateral rectus muscle and extraconal space** (black arrow) and **involvement of the infraorbital nerve (V_2)** (thin white arrow). (**c**) Axial T1 post-contrast MRI with fat saturation shows **enhancing tissue in the right pterygopalatine fossa** (arrow) and **involving the infraorbital nerve (V_2)** (thin arrow). (**d**) Axial T2 MRI without fat saturation shows **isointense right intraconal soft tissue** (arrow). (**e**) Axial ^{18}F-FDG PET/CT shows **FDG-avid disease in the right orbit** (arrow). (**f**) Axial ^{18}F-FDG PET/CT shows **FDG-avid disease involving the right infraorbital nerve** (arrow)

MRI

- **T1 hypointensity, T2 hypo- to hyperintensity with homogeneous enhancement** [47, 48, 50].
- IgG4-related **hypophysitis** has also been described with **thickened enhancement of the pituitary infundibulum** [51].

PET

- IgG4-RD is **^{18}F-FDG-avid,** and PET is useful to **detect multiorgan involvement, guide biopsies**, and **assess treatment response** [46, 52].

Key Points

- Assess for involvement of the **salivary glands**, e.g., parotid and submandibular glands.
- Assess for involvement of **cranial nerves** (e.g., **infraorbital nerve**), l**acrimal gland**, **extraocular muscles**, **cavernous sinus**, and Meckel's cave.
- Describe involvement and signs of **compression at the orbital apex**.

References

1. Newman SA, Jane JA. Meningiomas of the optic nerve, orbit, and anterior visual pathways. In: Al-Mefty O, editor. Meningiomas. New York, NY: Raven Press; 1991. p. 461–94.
2. Ortiz O, Schochet SS, Kotzan JM, Kostick D. Radiologic-pathologic correlation: meningioma of the optic nerve sheath. AJNR Am J Neuroradiol. 1996;17:901–6.
3. Parker RT, Ovens CA, Fraser CL, Samarawickrama C. Optic nerve sheath meningiomas: prevalence, impact, and management strategies. Eye Brain. 2018;10:85–99. https://doi.org/10.2147/EB.S144345.
4. Dutton JJ. Optic nerve sheath meningiomas. Surv Ophthalmol. 1992;37:167–83. https://doi.org/10.1016/0039-6257(92)90135-g.

5. Kanamalla US. The optic nerve tram-track sign. Radiology. 2003;227:718–9. https://doi.org/10.1148/radiol.2273010758.
6. Badr MA, Elkhamary SM, Al Sabbagh S, Al TA. Bilateral Optic Nerve Sheath Meningioma with Intracanalicular and Intracranial Component in a 25-year-old Saudi Patient. Middle East Afr J Ophthalmol. 2008;15:138–41. https://doi.org/10.4103/0974-9233.51990.
7. Mafee MF, Goodwin J, Dorodi S. Optic nerve sheath meningiomas. Role of MR imaging. Radiol Clin N Am. 1999;37:37–58, ix. https://doi.org/10.1016/s0033-8389(05)70077-4.
8. Zimmerman CF, Schatz NJ, Glaser JS. Magnetic resonance imaging of optic nerve meningiomas. Enhancement with gadolinium-DTPA. Ophthalmology. 1990;97:585–91. https://doi.org/10.1016/s0161-6420(90)32538-1.
9. Klingenstein A, Haug AR, Miller C, Hintschich C. Ga-68-DOTA-TATE PET/CT for discrimination of tumors of the optic pathway. Orbit. 2015;34:16–22. https://doi.org/10.3109/01676830.2014.959185.
10. Vay SU, Werner JM, Kabbasch C, Schmidt M, Drzezga A, Fink GR, et al. Uncovering an optic nerve sheath meningioma using 68Ga-DOTATATE PET/CT. Clin Nucl Med. 2021;46(9):e464–5. https://doi.org/10.1097/RLU.0000000000003619.
11. Taylor T, Jaspan T, Milano G, Gregson R, Parker T, Ritzmann T, et al. Radiological classification of optic pathway gliomas: experience of a modified functional classification system. Br J Radiol. 2008;81:761–6. https://doi.org/10.1259/bjr/65246351.
12. Millar WS, Tartaglino LM, Sergott RC, Friedman DP, Flanders AE. MR of malignant optic glioma of adulthood. AJNR Am J Neuroradiol. 1995;16:1673–6.
13. Gala F. Magnetic resonance imaging of optic nerve. Indian J Radiol Imaging. 2015;25:421–38. https://doi.org/10.4103/0971-3026.169462.
14. Listernick R, Darling C, Greenwald M, Strauss L, Charrow J. Optic pathway tumors in children: the effect of neurofibromatosis type 1 on clinical manifestations and natural history. J Pediatr. 1995;127:718–22. https://doi.org/10.1016/s0022-3476(95)70159-1.
15. Jahraus CD, Tarbell NJ. Optic pathway gliomas. Pediatr Blood Cancer. 2006;46:586–96. https://doi.org/10.1002/pbc.20655.
16. Jakobiec FA, Depot MJ, Kennerdell JS, Shults WT, Anderson RL, Alper ME, et al. Combined clinical and computed tomographic diagnosis of orbital glioma and meningioma. Ophthalmology. 1984;91:137–55. https://doi.org/10.1016/s0161-6420(84)34316-0.
17. Razek AA, Castillo M. Imaging lesions of the cavernous sinus. AJNR Am J Neuroradiol. 2009;30:444–52. https://doi.org/10.3174/ajnr.A1398.
18. Wippold FJ 2nd, Lubner M, Perrin RJ, Lämmle M, Perry A. Neuropathology for the neuroradiologist: Antoni A and Antoni B tissue patterns. AJNR Am J Neuroradiol. 2007;28:1633–8. https://doi.org/10.3174/ajnr.A0682.
19. Wilson MP, Katlariwala P, Low G, Murad MH, McInnes MDF, Jacques L, et al. Diagnostic accuracy of MRI for the detection of malignant peripheral nerve sheath tumors: a systematic review and meta-analysis. AJR Am J Roentgenol. 2021;217:31–9. https://doi.org/10.2214/AJR.20.23403.
20. Skolnik AD, Loevner LA, Sampathu DM, Newman JG, Lee JY, Bagley LJ, et al. Cranial nerve schwannomas: diagnostic imaging approach. Radiographics. 2016;36:1463–77. https://doi.org/10.1148/rg.2016150199.
21. Romano N, Federici M, Castaldi A. Imaging of cranial nerves: a pictorial overview. Insights Imaging. 2019;10:33. https://doi.org/10.1186/s13244-019-0719-5.
22. Kapur R, Mafee MF, Lamba R, Edward DP. Orbital schwannoma and neurofibroma: role of imaging. Neuroimaging Clin N Am. 2005;15:159–74. https://doi.org/10.1016/j.nic.2005.02.004.
23. Baehring JM, Betensky RA, Batchelor TT. Malignant peripheral nerve sheath tumor: the clinical spectrum and outcome of treatment. Neurology. 2003;61:696–8. https://doi.org/10.1212/01.wnl.0000078813.05925.2c.
24. Chung SY, Kim DI, Lee BH, Yoon PH, Jeon P, Chung TS. Facial nerve schwannomas: CT and MR findings. Yonsei Med J. 1998;39:148–53. https://doi.org/10.3349/ymj.1998.39.2.148.
25. Koga H, Matsumoto S, Manabe J, Tanizawa T, Kawaguchi N. Definition of the target sign and its use for the diagnosis of schwannomas. Clin Orthop Relat Res. 2007;464:224–9. https://doi.org/10.1097/BLO.0b013e3181583422.
26. Dewey BJ, Howe BM, Spinner RJ, Johnson GB, Nathan MA, Wenger DE, et al. FDG PET/CT and MRI features of pathologically proven schwannomas. Clin Nucl Med. 2021;46:289–96. https://doi.org/10.1097/RLU.0000000000003485.
27. Brown IS. Pathology of perineural spread. J Neurol Surg B Skull Base. 2016;77(2):124–30. https://doi.org/10.1055/s-0036-1571837.
28. Ong CK, Chong VF. Imaging of perineural spread in head and neck tumours. Cancer Imaging. 2010;10(1):S92–8. https://doi.org/10.1102/1470-7330.2010.9033.
29. Carter RL, Foster CS, Dinsdale EA, Pittam MR. Perineural spread by squamous carcinomas of the head and neck: a morphological study using antiaxonal and antimyelin monoclonal antibodies. J Clin Pathol. 1983;36(3):269–75. https://doi.org/10.1136/jcp.36.3.269.
30. Raghavan P, Witek ME, Morales RE. Imaging of complications of chemoradiation. Neuroimaging Clin N Am. 2022;32(1):93–109. https://doi.org/10.1016/j.nic.2021.08.012.
31. Saremi F, Helmy M, Farzin S, Zee CS, Go JL. MRI of cranial nerve enhancement. AJR Am J Roentgenol. 2005;185(6):1487–97. https://doi.org/10.2214/AJR.04.1518.
32. Fischbein NJ, Kaplan MJ, Jackler RK, Dillon WP. MR imaging in two cases of subacute denervation change in the muscles of facial expression. AJNR Am J Neuroradiol. 2001;22:880–4.
33. Barakos JA, Dillon WP. Lesions of the foramen ovale: CT-guided fine-needle aspiration. Radiology. 1992;182(2):573–5. https://doi.org/10.1148/radiology.182.2.1732985.
34. Moonis G, Cunnane MB, Emerick K, Curtin H. Patterns of perineural tumor spread in head and neck cancer. Magn Reson Imaging Clin N Am. 2012;20(3):435–46. https://doi.org/10.1016/j.mric.2012.05.006.
35. Debnam JM, Mayer RR, Chi TL, Ketonen L, Weinberg JS, Wei W, et al. Most common sites on MRI of intracranial neoplastic leptomeningeal disease. J Clin Neurosci. 2017;45:252–6. https://doi.org/10.1016/j.jocn.2017.07.020.
36. Fritzhand SJ, Esmaeli B, Sun J, Debnam JM. Primary disease sites and patterns of spread in cases of neurolymphomatosis in the orbit associated with lymphoma. Cancer Imaging. 2021;21:39. https://doi.org/10.1186/s40644-021-00409-3.
37. Mayer RR, Frankfort BJ, Strickland BA, Debnam JM, McCutcheon IE, Groves MD, et al. Leptomeningeal metastases presenting exclusively with ocular disturbance in 34 patients: a tertiary care cancer hospital experience. J Clin Neurosci. 2017;39:151–4. https://doi.org/10.1016/j.jocn.2017.01.024.
38. Grisariu S, Avni B, Batchelor TT, van den Bent MJ, Bokstein F, Schiff D, et al. Neurolymphomatosis: an International Primary CNS Lymphoma Collaborative Group report. Blood. 2010;115:5005–11. https://doi.org/10.1182/blood-2009-12-258210.
39. Rothfus WE, Curtin HD. Extraocular muscle enlargement: a CT review. Radiology. 1984;151:677–81. https://doi.org/10.1148/radiology.151.3.6546996.
40. Yuen SJ, Rubin PA. Idiopathic orbital inflammation: distribution, clinical features, and treatment outcome. Arch Ophthalmol. 2003;121:491–9. https://doi.org/10.1001/archopht.121.4.491.
41. Weber AL, Romo LV, Sabates NR. Pseudotumor of the orbit. Clinical, pathologic, and radiologic evaluation. Radiol Clin N Am. 1999;37:151–68, xi. https://doi.org/10.1016/s0033-8389(05)70084-1.

42. Li Y, Lip G, Chong V, Yuan J, Ding Z. Idiopathic orbital inflammation syndrome with retro-orbital involvement: a retrospective study of eight patients. PLoS One. 2013;8:e57126. https://doi.org/10.1371/journal.pone.0057126.
43. Umehara H, Okazaki K, Masaki Y, Kawano M, Yamamoto M, Saeki T, et al. Comprehensive diagnostic criteria for IgG4-related disease (IgG4-RD), 2011. Mod Rheumatol. 2012;22:21–30. https://doi.org/10.1007/s10165-011-0571-z.
44. Stone JH, Zen Y, Deshpande V. IgG4-related disease. N Engl J Med. 2012;366:539–51. https://doi.org/10.1056/NEJMra1104650.
45. Hayashi Y, Moriyama M, Maehara T, Goto Y, Kawano S, Ohta M, et al. A case of mantle cell lymphoma presenting as IgG4-related dacryoadenitis and sialoadenitis, so-called Mikulicz's disease. World J Surg Oncol. 2015;13:225. https://doi.org/10.1186/s12957-015-0644-0.
46. Fujita A, Sakai O, Chapman MN, Sugimoto H. IgG4-related disease of the head and neck: CT and MR imaging manifestations. Radiographics. 2012;32(7):1945–58. https://doi.org/10.1148/rg.327125032.
47. Himi T, Takano K, Yamamoto M, Naishiro Y, Takahashi H. A novel concept of Mikulicz's disease as IgG4-related disease. Auris Nasus Larynx. 2012;39(1):9–17. https://doi.org/10.1016/j.anl.2011.01.023.
48. Ginat DT, Freitag SK, Kieff D, Grove A, Fay A, Cunnane M, et al. Radiographic patterns of orbital involvement in IgG4-related disease. Ophthalmic Plast Reconstr Surg. 2013;29:261–6. https://doi.org/10.1097/IOP.0b013e31829165ad.
49. Mahalingam HV, Mani SE, Patel B, Prabhu K, Alexander M, Fatterpekar GM, Chacko G. Imaging spectrum of cavernous sinus lesions with histopathologic correlation. Radiographics. 2019;39:795–819. https://doi.org/10.1148/rg.2019180122.
50. Tiegs-Heiden CA, Eckel LJ, Hunt CH, Diehn FE, Schwartz KM, Kallmes DF, et al. Immunoglobulin G4-related disease of the orbit: imaging features in 27 patients. AJNR Am J Neuroradiol. 2014;35:1393–7. https://doi.org/10.3174/ajnr.A3865.
51. Caputo C, Bazargan A, McKelvie PA, Sutherland T, Su CS, Inder WJ. Hypophysitis due to IgG4-related disease responding to treatment with azathioprine: an alternative to corticosteroid therapy. Pituitary. 2014;17:251–6. https://doi.org/10.1007/s11102-013-0498-9.
52. Zhao Z, Wang Y, Guan Z, Jin J, Huang F, Zhu J. Utility of FDG-PET/CT in the diagnosis of IgG4-related diseases. Clin Exp Rheumatol. 2016;34:119–25.